國立臺灣大學獸醫專業學院獸醫所基礎組

碩士論文

Graduate Institute of Veterinary Medicine
School of Veterinary Medicine
National Taiwan University

Master Thesis

# 建立以次氯酸鈉引發腹膜纖維化之豬動物模式

# Establishment of Hypochlorite-Induced Porcine Model of Peritoneal Fibrosis

趙淳媛

Chun-Yuan Chao

指導教授：蔡沛學 博士

Advisor: Pei-Shiue Tsai, Ph.D.

中華民國 108 年 6 月

June 2019

doi:10.6342/NTU201903182

# 國立臺灣大學（碩）博士學位論文

# 口試委員會審定書

## 建立以次氯酸鈉引發腹膜纖維化之豬動物模式

## Establishment of Hypochlorite-Induced Porcine Model of Peritoneal Fibrosis

本論文係趙淳媛君 (R06629015) 在國立臺灣大學獸醫學系、所完成之碩（博）士學位論文，於民國 108 年 6 月 25 日承下列考試委員審查通過及口試及格，特此證明

口試委員：

_____（簽名）

（指導教授）

_____ _____

_____ _____

_____ _____

系主任、所長 _____（簽名）

# 中文摘要

腎衰竭患者依靠挽救生命的腹膜透析來促進廢物交換並維持身體狀況的穩定。然而，腹膜透析本身和腹腔內手術經常導致腹膜纖維化和器官沾黏，這會損害腹膜透析的效率或內臟器官的正常功能。儘管嚙齒動物模型已經為腹膜纖維化的發病機制提供了有用的線索，但牠們與人體的生理學和解剖學上的差異限制了牠們在後續評估治療效果時的應用。在這本論文中，我們首次透過腹腔注射次氯酸鈉，於 5 週齡仔豬建立腹膜纖維化的動物模式。我們證實腹腔注射 30ml / kg BW，0.1%-0.2%（0.1mM-0.2mM）次氯酸鹽可以成功誘導腹膜纖維化和內臟器官沾黏，其特徵是器官表面增厚，膠原沉積，腹側腹膜間皮破碎和α-SMA$^{+}$肌纖維母細胞的增殖/累積。為了進一步了解次氯酸鈉誘導的腹膜纖維化的分子致病機制，我們以時間軸實驗來追蹤次氯酸鈉所引發之纖維化過程其細胞與分子層面的變化。在此實驗中，急性炎性細胞因子，IL-1$\beta$，TNF-$\alpha$，TGF-$\beta$1 和趨化因子 CX3CL1 在 0.1%SHC 處理的豬中有顯著上升的趨勢。通過此論文中建立的腹腔鏡檢查和活組織檢查與採樣，我們可以即時監測活體動物中器官纖維化和沾黏的進展與嚴重程度，並評估藥物及幹細胞預防與治療的效果，並且進行即時調整。此模型不僅可以用作研究纖維化形成的平台，還可用於評估藥物與再生醫學功效的動物模式。



doi:10.6342/NTU201903182

關鍵詞：豬模型，PF，腹膜透析，器官沾黏，細胞因子



doi:10.6342/NTU201903182

# Abstract

Patients with kidney failure rely on life-saving peritoneal dialysis (PD) to facilitate waste exchange and maintain homeostasis of physical conditions. However, PD itself and intra-abdominal surgery often result in peritoneal fibrosis (PF) and organ adhesions that compromise the efficiency of peritoneal dialysis or normal functions of visceral organs. Although rodent models had delivered useful clues on the pathogenesis of peritoneal fibrosis, their physiological and anatomical dis-similarities to human limit their further applications on the evaluation of therapeutic efficacy. In this thesis, we established for the first time, porcine model of peritoneal fibrosis by the use of a bleach-like chemical, sodium hypochlorite. We demonstrated that intraperitoneal injection of 30ml/kg B.W., 0.1%-0.2% (0.1mM-0.2mM) hypochlorite induced peritoneal fibrosis and visceral organ adhesions characterized by organ surface thickening, collagen deposition, ventral peritoneal mesothelium fragmentation, and $\alpha$-SMA$^{+}$ myofibroblasts proliferation/accumulation in 5-week-old piglets. To further understand the underlying mechanism of sodium hypochlorite-induced PF, we designed a time course experiment to follow the progression of this fibrosis model. In this experiment, acute inflammatory



doi:10.6342/NTU201903182

cytokine, IL-1β, TNF-α, TGF-β1 and CX3CL1 chemokine was significant elevated in 0.1% SHC-treated pigs. With laparoscopy examination and biopsy established in current study, we could monitor the progression and severity of organ fibrosis and adhesion in alive animals and evaluate the efficacy of preventive and/or therapeutic treatments with possibility of instant adjustments. This pig model could not only be used as a platform for studying fibrosis/scar formation, but can also be used to evaluate the efficacy of potential candidates on the prevention (e.g. compounds) and treatments (e.g. stem cells) for regenerative medicine.

**Keywords**: porcine model, PF, peritoneal dialysis, adhesion, cytokine



doi:10.6342/NTU201903182

# Contents





doi:10.6342/NTU201903182

doi:10.6342/NTU201903182

doi:10.6342/NTU201903182

# List of Figures





doi:10.6342/NTU201903182

doi:10.6342/NTU201903182

# List of Tables





doi:10.6342/NTU201903182

# Chapter 1 Introduction

## 1.1 General peritoneal structure and its physiological functions

Peritoneum, a large membrane lining the abdominal cavity, connects and supports most of the visceral organs. The peritoneum consists of two continuous parts, parietal and visceral peritoneum (Fig. 1). Both types are composed of simple squamous epithelial cells called mesothelium with subjacent submesothelial layer containing loose connective tissue, blood vessels, lymphatic vessels and nerves[11]. The parietal peritoneum lines on the internal surface of abdominal cavity while visceral peritoneum covers the majority of the visceral organs.

The peritoneum is known to have multiple functions. For example, it prevents friction between adjacent organs by secreting serum which acts as a lubricant. Another function of peritoneum is that it holds the internal organs at their proper positions; moreover, peritoneum controls the small molecular exchange between bloodstream and abdominal cavity through its semipermeable characteristics[7].

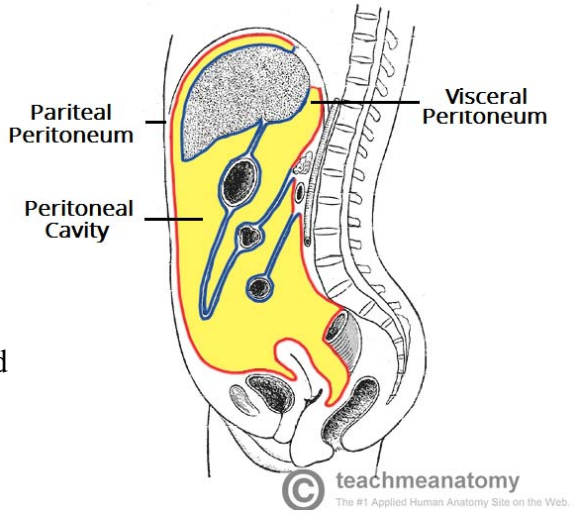


**Figure 1** The structure of peritoneum and the peritoneal cavity
[2]



doi:10.6342/NTU201903182

## 1.2 Peritoneal injury

### 1.2.1 Causes of peritoneal injury

Causes of peritoneal injury are varied, among all, peritonitis is one of the most commonly seen causes of peritoneal injury. Many of the peritonitis cases are seen in post-operation complications or as a consequence of long-term peritoneal dialysis (PD) [36]. PD is one of the life-saving treatments for patients with kidney failure based on the ultrafiltration ability of peritoneum to eliminate the waste product and superfluous ions from bloodstream (Fig. 2)[6]. Although the survival of PD patients is superior to that of haemodialysis patients during the first year of PD[5]. PD itself may lead to peritonitis or further develop into peritoneal fibrosis (PF) [34]. A variety of insults, including bioincompatible dialysates (acidic solution, high glucose contains, glucose degradation products or combination of all above-mentioned), different causes of peritonitis, uremia and chronic inflammation have been reported to cause peritoneal injury [8,45]. No matter what are the causes of peritoneal injury, the common consequences is the damages of mesothelium layer and ultrafiltration failure and eventually PD treatment failure.



doi:10.6342/NTU201903182

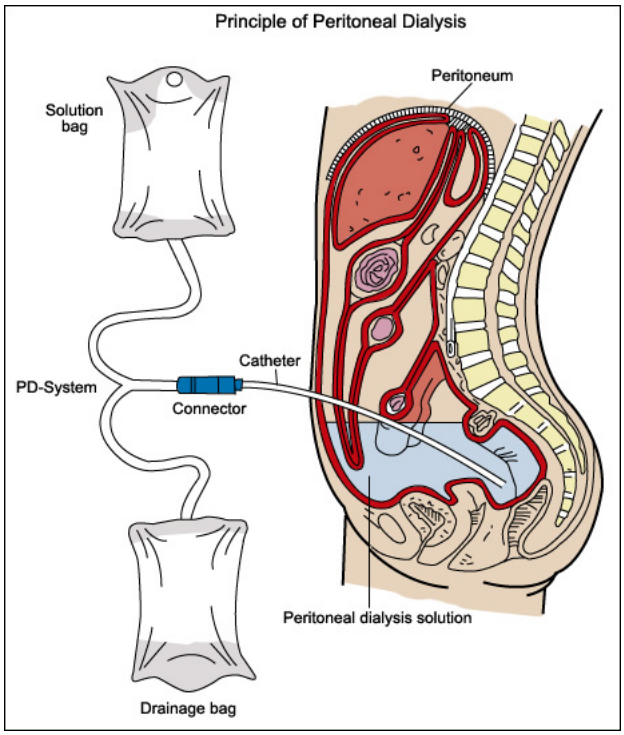


**Figure 2** Principle of peritoneal dialysis
[1]

### 1.2.2 Clinical signs for peritonitis

One of the clinical manifestations for peritonitis is ultrafiltration failure and can occur in up to 30% of patients after five years of PD [17]. Ultrafiltration failure occurs due to acceleration of small-solute transport dissipating the necessary osmotic gradient to maintain fluid balance. The most common symptoms of peritonitis among PD patients are abdominal pain and cloudy peritoneal effluent, other symptoms also include fever, nausea and diarrhea. [39]. To evaluate the development and causes of peritonitis in PD patients, the peritoneal fluid should be analyzed for cell count, cell types, and differential diagnosis should also be carried out with gram stain and further culture. As for the evaluation on the function of peritoneal membrane, the peritoneal equilibration



doi:10.6342/NTU201903182

test can be applied [41,47]. It is a semiquantitative assessment of peritoneal membrane transport function by assess the solute transport rate of their equilibration between the peritoneal capillary blood and dialysate.

In addition to ultrafiltration failure, clinical signs, such as severe malnutrition, intestinal occlusion and ascites have also been suggested for the presence of encapsulated peritoneal sclerosis (EPS), a rare but lethal complication resulted from severe peritoneal injury [8]. EPS is associated with extensive thickening and fibrosis of the peritoneum resulting in the formation of a fibrous cocoon encapsulating the bowel leading to intestinal obstruction. The fibrous cocoon gradually covers the intestines and leads to malnutrition, weight loss, bowel obstruction, ischemia and strangulation, infection and eventually, the death of patients [35].

Various cytokines, such as IL-1, IL-6, transforming growth factor-beta(TGF-β) have been correlated with peritonitis[26]. For TGF-β1, it is a multifunctional peptide that controls proliferation, differentiation, and other functions in many cell types [14]. A wide range of animal studies have established TGF-β1 as the predominant pathogenic factor or ‘master regulator’ that drives glomerular and tubulointerstitial fibrosis [34]. Overexpression of the active form of TGF-β1 is sufficient to induce fibrotic disease in multiple organs, including the kidney and peritoneal membrane[32,33,42].



doi:10.6342/NTU201903182

### 1.2.3 Pathological findings

The most common pathological findings indicating peritoneal injury are fibrin deposition, loss of mesothelial cells (MCs), thickening of extracellular matrix (ECM) in submesothelial compact zones, hyalinizing vasculopathy and angiogenesis (Fig. 3)[10,54]. Some reports suggested that MCs can undergo epithelial-to-mesenchymal transition (EMT) after injury, transformed MCs are thus able to produce ECM and lead to excessive accumulation of ECM, resulting in the observed fibrosis [3]. EMT process can be characterized by the expression of α-smooth muscle actin (αSMA) and cytokeratin simultaneously by cells located in the submesothelial compact zone (Fig. 4)[6]. However, other study using lineage tracing analysis in mouse model questioned the transformation of MCs and the occurrence of EMT process upon the development of PF, from that recent study, authors suggested that submesothelial fibroblast are the major source of myofibroblasts in PF and surviving MCs are the principal cells for remesothelialization after injury[5].



doi:10.6342/NTU201903182

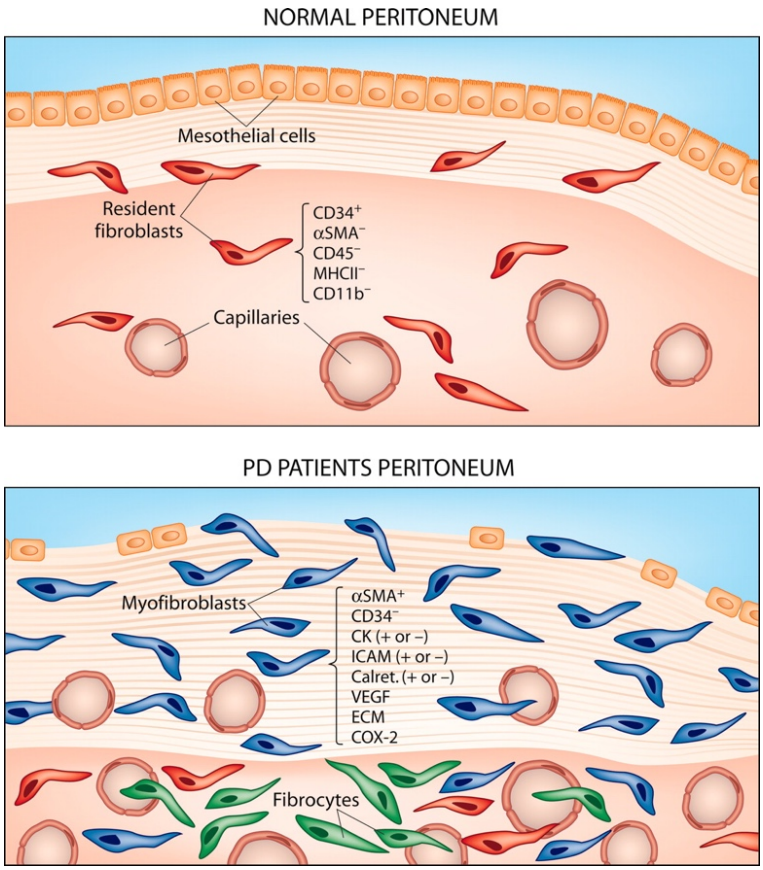


**Figure 3** Cell population in peritoneal membrane of normal and PD patients [4]

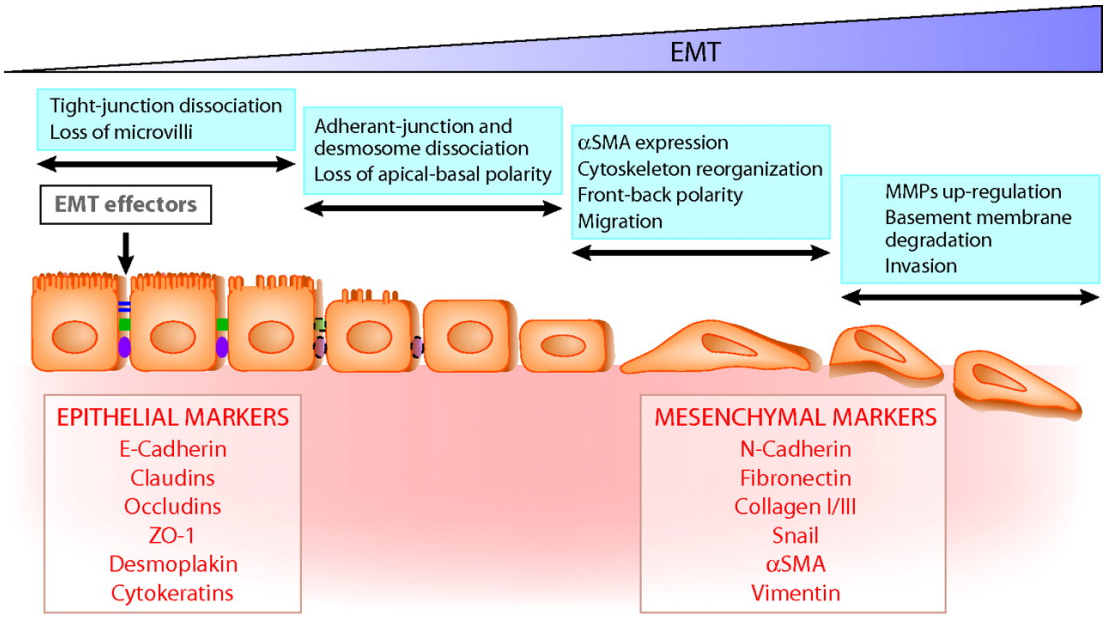


**Figure 4** Key events during EMT [4]



doi:10.6342/NTU201903182

## 1.3 Animal models for the study of peritoneal dysfunction

### 1.3.1 Rodent models (Advantages/Disadvantages/Similarity)

To overcome problems and complications mentioned above, therapeutic intervention, biocompatible PD solution and pharmaceutical agents need to be tested before applying on clinical practice. Although experimental procedures or trails carry out on humans may provide the definite answer for these concerns, it is however complicated by technical and ethical issues. Luckily, based on the similar transportation characteristics of solute and water across the peritoneal membrane in most mammals, a variety of experiment and tests can therefore be performed and pre-evaluated in different animal models prior to pre-clinical human trials. Rodent species such as rats and (genetically modified) mice most commonly used experimental models for the evaluation on the severity of peritoneal injury and/or the efficacy of potential treatments. The advantages of these rodent species as animal model for the study of peritoneal injury including easy to handle, relatively low cost for the maintenance and breeding, fast generation time (on average 21 days of pregnancy length); moreover, complete information on the gene background provides full potential on the genetic manipulations when specific gene, molecule or protein is identified. However, their short life expectancy, limited abdominal volume, and dis-similar genomic responses poorly mimic human inflammatory diseases[45] which increase the difficulties for operation and the



doi:10.6342/NTU201903182

interpretation of experimental data when applied to human patients.

### 1.3.2 Porcine model (Advantages/Disadvantages/Similarity)

When compare with rodent species, porcine is a suitable animal species for modeling human diseases in terms of their organ size, anatomical and physiological similarities. Moreover, longer life expectancy, the closer immune system to human and predominantly human-like responses toward inflammation can yield better understanding than information obtained from rodent species[9]. Due to these advantages, pigs have been widely use as animal models to mimic human diseases, particularly for the study of cardiovascular disease[16], hepatic cirrhosis[51], wound repair[44], diabetes[12], ophthalmology[38], respiratory medicine[23] and kidney transplantation[25]. As for modeling inflammation, Renner et al. demonstarted that pig is an excellent and superior mammalian model to study the mechanisms involved in acute and chronic intestinal injury and inflammation, as the intestine is anatomically and functionally similar to the human intestine[50]. Another advantage of porcine species is that when compare with rodent species, pig can tolerate more complex and repeated surgery when necessary. However, one of the most challenging issues of using pig as animal model is their high costs on breeding, maintenance and difficulty on handling throughout the experiments.



doi:10.6342/NTU201903182

### 1.3.3 Animal models of other species (Advantages/Disadvantages /Similarity)

Other animals such as rabbits, dogs, sheep or even kangaroos [49] have been used for the study of peritoneal injury. Rabbit [15]can survive longer on PD and the operation is easier than in rodents, but rabbits are delicate animals that can have high mortality rate during the experimental procedure. Other animals, such as dogs, sheep that have been used for the study of peritoneal injury shared similar life expectancy and can be used to operate PD easier than rodent; however, their availability and their difficulties in the maintenance and breeding often limited their used as a common animal model for human diseases.

## 1.4 Methods to induce peritoneal dysfunction in animal model

For experimentally-induced peritoneal fibrosis, several approaches have been established, these including (1) PD solution with glucose degradation product [43] . A study showed that the damage of the peritoneal membrane induced by glucose degradation products is mediated by the activation of advanced glycation end-products receptor.[43] (2) Bacterial (Staphylococcus sp.)[20] . Use of the bacteria itself and/or culture supernatant to induce peritoneal fibrosis are characterized with apparent gross adhesion, increased connective tissue and collagen deposit. (3) Peritoneal TGF-β1 overexpression [32,33]. Several studies showed that transient overexpression of TGF-



doi:10.6342/NTU201903182

β1 induced epithelial mesenchymal transition in the rodent peritoneum and resulted in peritoneal fibrosis. (4) Chemical irritants [19,27]. For example chlorhexidine [24], povidone iodine [30], formaldehyde [31], chlorhexidine gluconate [21], acidic (pH 3.5) solution [37] and sodium hypochlorite(SHC) [27] have been used as chemical irritants to induce PF, among above-mentioned compounds, SHC is one of the most commonly used irritants to establish the chemical-induced peritonitis base on its convenience in usage and reproducibility of results. However, whether these chemical-induced PF share the same or similar pathogenesis with other causes remain unclear.

## 1.5 Aim of this study

In this study, we aim to establish hypochlorite-induced PF in pig and provide comprehensive evaluation methods including ante-mortem laparoscopy examination and biopsy, post-mortem necropsy and pathological evaluation to assess peritoneum integrity, collagen deposition, thickening of SM compact zone and (myo)fibroblast accumulation. Besides establishment of porcine model of PF, in this study, we will also investigate the underlying mechanism of sodium hypochlorite-induced PF, to follow the progression and development of SHC-induced PF, a time course experiment and analyses of local (peritoneal cavity) and systemic (serum) responses will be performed. By establishing novel porcine model of PF and understand the pathogenesis of this model, we can accelerate efficacy evaluation of target compounds, pre-clinical



doi:10.6342/NTU201903182

therapeutic trail assessments and provide a common evaluation platform for validating findings from murine models as well as accessing feasibility, efficiency and clinical safety of regenerative cell therapy prior to human trials.



doi:10.6342/NTU201903182

# Chapter 2 Materials and Methods

## 2.1 Chemicals, reagents, antibodies

Chemicals and reagents were obtained from Sigma Aldrich (USA) unless otherwise stated. Rabbit polyclonal anti-human Cytokeratin Clones AE1/AE3 was obtained from Dako (Agilent, USA). Goat polyclonal anti-alpha smooth muscle actin, rabbit polyclonal anti-TGF beta 1 and Rabbit polyclonal anti-CX3CL1 were purchased from Abcam (UK). IL1-β and TNF-α ELISA kits were obtained from R&D Systems Inc. (USA). TGF-β1 ELISA kit was from BosterBio (Canada).

## 2.2 Establishment of SHC-induced pig model

### 2.2.1 End point model

Animal experiments were approved and carried out under the regulation and permission of IACUC protocols (NTU-106-EL-00165) at National Taiwan University (NTU, Taiwan). Four-week-old domestic piglets (obtained from Tung-Ying Agriculture Inc.) that were free from porcine epidemic diarrhea virus (PEDV), porcine reproductive and respiratory syndrome virus (PRRSV) and porcine circovirus (PCV) (tested with PCR, data not showed) were housed for 3-5 days prior to the experiments in a certified and approved animal facility. On the day of experiment, piglets were weighted and sedated by intramuscular (IM) injection of xylazine (2 mg/kg) and tiletamine/zolazepam (4 mg/kg) mixture. Basic physiological parameters such as breath, heart rate, body



doi:10.6342/NTU201903182

temperature, blood oxygen level, blood pressure and electrocardiogram (EKG) were monitored. To establish a sodium hypochlorite-induced PF in pigs, injection of SHC (Sigma-Aldrich, USA) was performed according the method described in mouse with some modifications[5]. Briefly, 30 ml/kg B.W. (~300 ml/pig) sterilized normal saline contained 0% (v/v), 0.05% (v/v, 7.5 mM), 0.1% (v/v, 15 mM) and 0.2% (v/v, 30 mM) chemical irritant; SHC was given intraperitoneally (Fig. 6A1-3). Pre- and post-SHC injection ultrasonography examinations were carried out (Fig. 5) and pigs were closely monitored by certified veterinarians at a daily basis (Fig. 6A4).

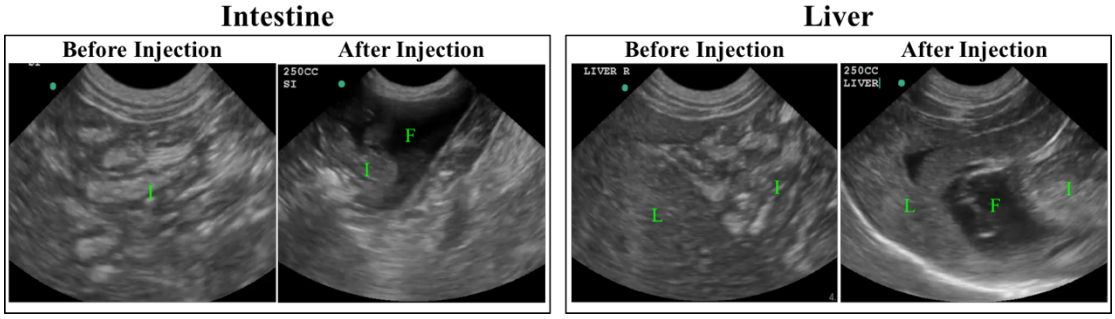


**Figure 5** Ultrasongraphy confirmed the injection of hypochlorite into abdominal cavity Ultrasongraphy was used to monitor the injection of hypochlorite. Pre-injection evaluation was carried out thoroughly for the comparison with post-inject analysis. I: intestine; L: liver; F: injected fluid (hypochlorite).

### 2.2.2 Time course progression model

To further understand the progression and identify potential cellular mechanism of SHC-induced PF, a time course SHC model was performed based on 0.1% SHC treatment. After pigs were housed in the animal facility as descried above, they were randomly assigned to three groups (n=3 in each experimental group, 9 pigs in total),



doi:10.6342/NTU201903182

and were sacrificed on day 2, 4,7 post SHC injection (day 0). To establish the basal value of all parameters, five days before the injection of SHC (day -5), blood samples and abdominal lavage fluid were collected. Animals were anesthetized as described above and peritoneal cavity was infused with 10 ml/kg sterile saline. Each pig received a 1-min gentle manual massage and infused fluid (>50 ml) containing secretion (e.g. cytokines) from tissues, cell debris were collected. All pigs were injected with SHC at day 0, and on day 2, 4, 7 post injection, bloods samples and lavage fluid were also collected immediately after sacrificed. Tissue sample (abdominal wall, liver, duodenum, omentum) were also collected upon necropsy.

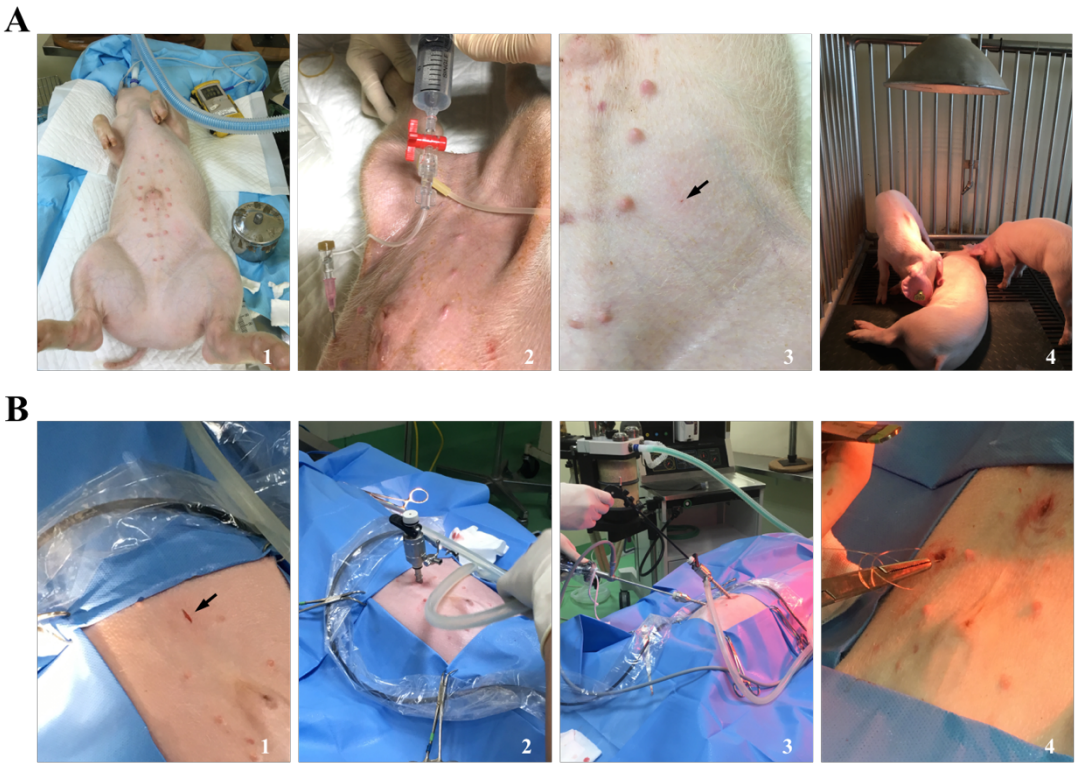


**Figure 6** Operation of hypochlorite-injection and antemortem laparoscopy evaluation of peritoneal fibrosis
(A) Hypochlorite was diluted with sterilized saline and was administrated via



doi:10.6342/NTU201903182

intraperitoneal injection in anesthetized pigs (1-2). Injection site was indicated with arrow (3). Pigs were placed in a high stand recovery room with heated lamp after hypochlorite injection (4). (B) Antemortem laparoscopy evaluation of peritoneal fibrosis was carried out as described in methods and material under aspectic condition. Incision site was marked with arrow.

## 2.3 Antemortem laparoscopy evaluation

To establish antemortem evaluation to monitor the development of PF, laparoscopic examination was conducted one week after SHC administration. In brief, pigs were premedicated with xylazine and tiletamine/zolazepam intramuscularly at dose of 2 mg/kg and 4 mg/kg, respectively. Twenty-four-gauge intravenous (IV) catheter was placed in lateral auricular vein of the ear for peri-operative administration of iv medication. The trachea was intubation and general anesthesia was maintained in pigs with 1-3% isoflurane in oxygen. The core body temperature was maintained between 36°C to 38°C by forced-air warming device. The vital signs, respiratory pattern, blood pressure, EKG, and end-tidal carbon dioxide ($CO_2$) were monitored continuously. Normal saline was infused intravenously at a rate of 5 ml/hr/kg. Positive pressure ventilation was given during laparoscopy examination. The pigs were placed in dorsal recumbence (Fig. 6B1). After aseptical preparation, pneumoperitoneum was achieved by infusing $CO_2$ via a Veress needle (Fig. 6B2). A two-port technique was adopted for laparoscopic exploration and biopsy. A 5-mm laparoscope was introduced into abdominal cavity through one of the trocars. The laparoscopic instruments, such as



doi:10.6342/NTU201903182

palpating probe and biopsy cup forceps were introduced through the other trocar (Fig. 6B3). In the exploratory, 360-drgree endoscopic examination was performed to inspect the whole peritoneal condition (Videos). To evaluate the degree of PF, laparoscopic biopsies of liver and ventral peritoneum were collected by biopsy cup forceps for histopathological examinations. All biopsied sites were monitored for bleeding. As soon as hemostasis of biopsied site had verified, the insufflation of $CO_2$ was stopped. Before cannula removal, intra-abdominal $CO_2$ was purged from the peritoneal cavity. Port closure was achieved by placing 3-0 monofilament absorbable sutures (monosyn) into the muscle fascia of the body wall followed by the subcutaneous tissue. Skin incision was opposed and closed with tissue glue (Fig. 6B4).

## 2.4 Tissue preparation, pathological evaluation and immunohistochemistry staining (IHC)

After pigs were sacrificed, the severity of PF and adhesions of visceral organs were scored according to the gross adhesion scoring system previously reported with some modifications[13]. Modified necropsy scoring system was shown in table 1. Tissues, including liver, mesentery, intestine, omentum and abdominal wall, were collected for pathological analyses. Tissues were fixed in 10% neutral formalin for overnight and processed for paraffin embedding. Five-μm tissue sections were stained with hematoxylin and eosin (H&E) for general morphological and pathological evaluations.



doi:10.6342/NTU201903182

Masson's trichrome and collagen type I stain were carried out for collagen deposition evaluation. Based on H&E stained tissue sections, pathologic scoring was performed using a triple blind method by 3 independent certified pathologists. The relative severity of lesions and inflammation was graded on a 0 to 3 scale and total pathologic scoring was expressed as the sum of each parameter. Overall lesion scoring was calculated as the sum of all parameters examined. For tissue fibrosis analysis, Masson's trichrome stained sections were quantitatively assessed using CellSens software (Olympus, Tokyo, Japan) and the thickness of deposited collagen was measured manually in each sample. For immunohistochemistry staining, paraffin-embedded tissue sections were used. After the deparaffinized and rehydration procedures with xylene and ethanol (100-80%), the slides will be submerged in commercially available trilogy (Sigma-Aldrich, USA) and heated to 121ºC for 3 min in autoclave and cool down to 45ºC for antigen retrieval. Endogenous peroxidase was removed by submerging the slides into 3% $H_2O_2$ (diluted with pure methanol). After blocking by 1X normal goat serum (diluted with PBS, Jackson ImmunoResearch Laboratories Inc. PA, USA) for 1 hr at room temperature (RT), antibodies against specific protein of interests were applied to the tissues for overnight incubation at 4ºC. Leica Novolink Plymer Detection System (Leica, Solms, Germany) were used to generate positive signals followed the manufacturer's instruction. Slides were subsequently counterstained with hematoxylin



doi:10.6342/NTU201903182

and sealed with coverslips for evaluation and quantification.

**Table 1** Gross pathological scoring system

| Organ | Description | | Score |
|---|---|---|---|
| Liver | Normal | | 0 |
| | Dull edge | | 1 |
| | Surface turbid thickening | Local | 2 |
| | | Diffuse | 3 |
| | Fusion of lobes | | 4 |
| Spleen | Normal | | 0 |
| | Irregular surface | | 1 |
| | Surface turbid thickening | Local | 2 |
| | | Diffuse | 3 |
| Intestine | Normal | | 0 |
| | Surface turbid thickening | | 1 |
| | Adhesion | Mild | 2 |
| | | Severe (multiple loops) | 3 |
| Adhesions of visceral organs | No adhesion | | 0 |
| | Peritoneum adhesion with liver | | 2 |
| | Peritoneum adhesion with spleen | | 2 |
| | Peritoneum adhesion with intestine | | 2 |
| | Liver adhesion with spleen | | 2 |
| | Liver adhesion with intestine | | 2 |



doi:10.6342/NTU201903182

## 2.5 Indirect immunofluorescence staining and image acquisition

For indirect immunofluorescent assay (IFA), to obtain maximum information, a thicker section of 10 μm paraffin-embedded tissue sections were deparaffinized, rehydrated and underwent antigen retrieval as above-mentioned. After blocked with 1% BSA for 30 min at RT, tissue sections were further permeabilized with 100% ice-cold methanol at -20ºC for 10 min. Primary antibodies incubation was carried out with overnight incubation at 4ºC. After intense washed, sections were subsequently incubated with secondary antibodies for 1.5 hr at RT. Stained sections were mounted with Vectashield in the presence of diamidino-2-phenylindole (DAPI, Vector Lab, Peterborough, UK). As for negative controls, each immunoreaction was accompanied by a reaction omitting the primary antibody. All samples were evaluated with either Olympus IX83 epifluorescence microscopy or with Leica TCS SP5 II confocal scanning microscopy and analyzed with ImageJ (NIH) or CellSens software (Olympus, Tokyo, JP). Background subtraction and contrast/ brightness enhancement (up to ~20% enhancement using the maximum slider in both software) were performed identically for all images (including control images) in the same experiment.

## 2.6 Tissue surface thickening, mesothelial cells integrity and alpha smooth muscle actin (α-SMA) quantification



doi:10.6342/NTU201903182

To quantify surface thickening of the tissues under SHC stimulation, an objective multipoint measurement on the surface thickness was performed using ImageJ software as described by Su et. al[46]. For mesothelial cell integrity evaluation, cytokeratin was used. A mosaic tile image for the entire tissue sampled was first generated. The length (in μm) of the (1) total tissue surface and (2) $CK^+$ region in length were measured (Fig. 7). A ratio of ($CK^+$ length /total tissue surface length) was calculated and expressed in percentage. To quantify the amount of myofibroblast, specific marker protein α-SMA was used, total signal intensity (in pixel) was calculated and signals from the blood vessel were manually selected and removed. The quantity α-$SMA^+$ signal was expressed as positive pixel/$\mu m^2$ tissue area.

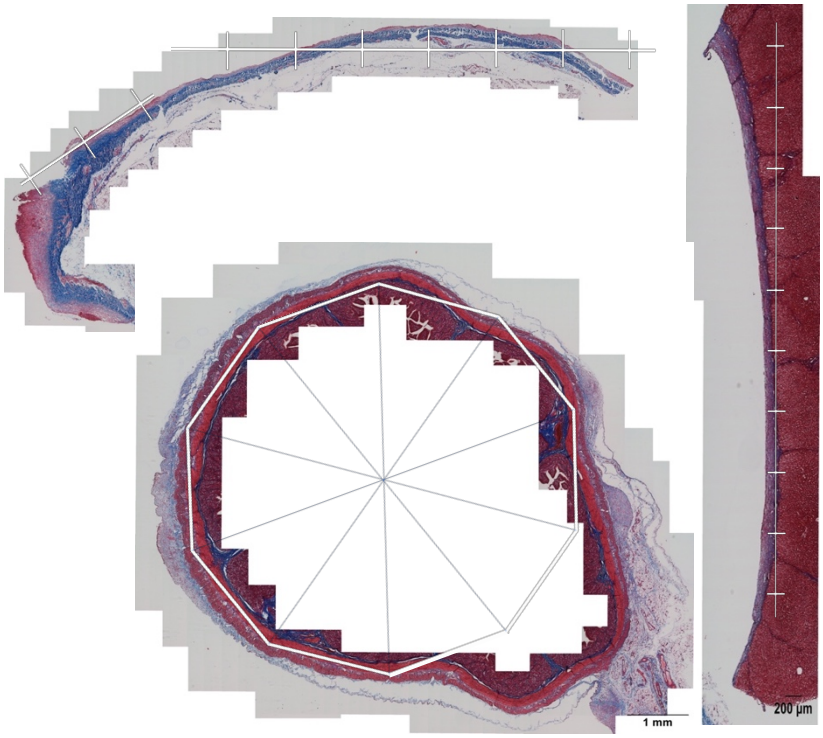


**Figure 7** Schematic diagram of measurement points
10 equally distributed measurements were quantified on each sample.



doi:10.6342/NTU201903182

## 2.7 Enzyme-linked immunosorbent assay (ELISA) analysis

To examine cytokine production in the circulation (from serum samples) and local area (from abdominal lavage samples) after SHC stimulation, target specific ELISA was performed on serum samples and abdominal lavage fluid from either end point samples or from time course groups. Both serum and abdominal lavage samples were centrifuged at 1450 G for 30 min at 4 ºC, and supernatant was collected; supernatants from lavage samples were further concentrated with Amicon Ultra-15 3Kdevice (Merck, Germany) to achieve a ~10 fold concentrated abdominal fluid. Serum and concentrated lavage samples were freezed at -80 ºC for later cytokine assessment.

Commercially available ELISA kits from R&D Systems Inc. (USA) were used per manufacture's guidelines. In brief, for ELISA analysis, flat-bottomed Nunc Maxisorp plates were coated with 100 μl of relevant capture antibody (e.g.IL1-β and TNF-α) overnight at RT. Following three washes with PBS containing 0.05% Tween-20 (PBST), plates were blocked with 300 μl of 1% BSA in PBS at RT for 1 hr. After plates were washed with PBST, 100 μl of recombinant antigen (used as standard) and samples from experimental animals were added and incubated for 2 hr at RT. After three washes with PBST, 100 μl of detection antibody were added and further incubate for 2 hr at RT. For signal detection, 100 μl Streptavidin-HRP were added and incubated for 20 min before reading with full wavelength ELISA reader (EMax® Plus Microplate



doi:10.6342/NTU201903182

Reader, Molecular Devices, Taiwan).

To detect TGF-β1, available ELISA kits from Boster (Canada) were used. Samples were activated by adding 20 μl of Solution A (1 N HCl) into 100 μl of sample, 10 min later, adding 20 μl of Solution B (1.2 N NaOH/0.5 M HEPES). The following steps were based on manufacture's guidelines.

## 2.8 Real-time PCR

Real-time PCR was performed using SYBR Advantage qPCR Premix (TaKaRa, Japan). Each real-time PCR reaction (20 μl) contained 3 μl of diluted reverse transcription product, 0.5 μl of forward and reverse primers, and 12.5 μl of SYBR Advantage qPCR Premix. To evaluate mRNA level of the tested cytokines, specific primers were used (Table. 2). For quantification, standard curves consisting of serial dilutions of the appropriate cDNA were included. The following PCR protocol were used for TGFβ1, glyceraldehyde-3-phosphate dehydrogenase (GAPDH): samples were denaturation for 15 sec at 95 ºC, followed by 40 cycles of 5 sec of denaturation at 95 ºC and 30 sec of annealing and elongation at 59 ºC. After each PCR reaction, melting curves were obtained by step- wise increases in the temperature from 60 ºC to 95 ºC to ensure single-product amplification. Negative control was prepared with the same protocol but without cDNA in the reaction mixture. To confirm the specificity of RT-PCR products, gel electrophoresis was also conducted. Raw reading values obtained from the real-time



doi:10.6342/NTU201903182

PCR were normalized with GAPDH and expressed as fold change to control animals.

**Table 2** Primers used for real-time PCR

| Gene | Sequence (5'–3') | Product size | EMBL/Reference |
|---|---|---|---|
| TGF-β1 | Forward: GGA AAG CGG CAA CCA AAT<br>Reverse: TCT GCC CGA GAG AGC AAT ACA | 120 | AF281156 / [4] |
| GAPDH | Forward: CCT TCA TTG ACC TCC ACT ACA TGG T<br>Reverse: CCA CAA CAT ACG TAG CAC CAC GAT C | 183 | U48832 / [48] |



doi:10.6342/NTU201903182

# Chapter 3 Results

## 3.1 Antemortem laparoscopic examination revealed fibrotic organ surface and tissue adhesions in SHC-treated pigs

Pre-injection ultrasoundgraphy (Fujifilm SonoSite, USA) examination was carried out to assess the (ab)normality of peritoneal cavity of pigs. Administration of SHC was then monitored by ultrasonography, an apparent anechoic area (marked as ‘F” for injected fluid) was observed between liver and intestine after SHC injection (Fig 5). Antemortem evaluation of PF was carried out by laparoscopic examinations one week after intraperitoneal (ip) administration of SHC (Supplementary videos 1-4). While no apparent gross lesions were observed in control (saline) and 0.05% SHC-treated pigs (Supplementary videos 1-2), dose-dependent severity of gross lesions, including liver capsule thickening (marked with arrow heads), multifocal adhesions of liver capsule with abdominal wall or serosa of intestine were observed (marked with arrows) in pigs treated with 0.1 and 0.2% SHC (Fig. 8A, Supplementary videos 3-4). Liver biopsy samples obtained upon laparoscopy evaluation revealed a normal liver histology in control pig; however, proliferation of fibrous connective tissue at the surface of liver with occasionally, few lymphocytes infiltration was observed in liver biopsy obtained from pigs treated with 0.1 and 0.2% SHC (Fig. 8B).



doi:10.6342/NTU201903182

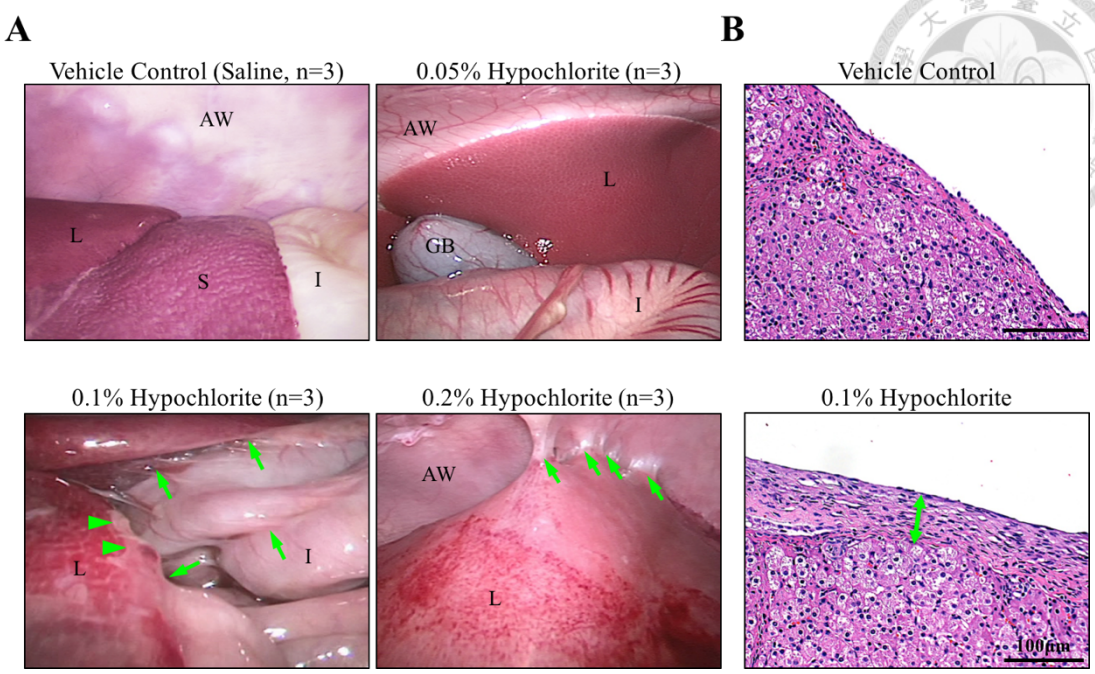


**Figure 8** Ante-mortem laparoscopy evaluation of abdominal cavity
**A.** Laparoscopy evaluation of abdominal cavity showed multi-point adhesions between abdominal wall and fibrotic visceral organs. **B.** Evaluation of abdominal fibrosis in liver biopsy obtained during laparoscopic evaluation. Accumulation of spindle-shape cells with an increased thickness (indicated with double-headed arrow bar) was observed at the surface of the liver from 0.2% SHC-treated pigs. L: liver; I intestine; GB: gall bladder; S: spleen; Aw: abdominal wall; green arrows indicated adhesions between visceral organs or between abdominal wall with organs; green arrowheads indicated fibrotic appearance on the surface of the organs. Bars represent 100 μm. Representative images from 3 individual pigs of each group were presented.

## 3.2 Pathology findings

### 3.2.1 Postmortem examination showed dose-dependent pathological changes after SHC stimulation

To provide a comprehensive and quantitative analyses of abdominal lesions, all pigs were euthanized one-week after the treatments and necropsy was performed. Grossly, as compared with saline-treated control pigs, no apparent gross lesion was noted in



doi:10.6342/NTU201903182

0.05% SHC-treated pigs (Fig. 9A). However, different levels of multifocal tissue adhesions (marked with arrows) characterized by turbid thickening of hepatic or splenic capsule, adhesion of peritoneal organs to organs, fusion of liver lobes, or adhesion of intestinal loops were noted in 0.1% and 0.2% SHC-treated pigs (Fig. 9A). Moreover, in 0.1 and 0.2% SHC-treated pigs, considerable amount of white fibrotic depositions was observed at the surface of visceral organs (marked with arrow heads). The pathological scoring result revealed that lesions in 0.1 and 0.2% SHC-treated pigs were 9.67±1.27 and 11.0±2, respectively (Fig. 9B), and were statistically more severe than that of saline- and 0.05% SHC-treated pigs (which scored as 1.25±0.14 and 0.83±0.53, respectively, Fig. 9B). The most severe lesions were noted in 0.2% SHC-treated pigs although not significantly difference was noted between 0.1% and 0.2% SHC-treated pigs.



doi:10.6342/NTU201903182

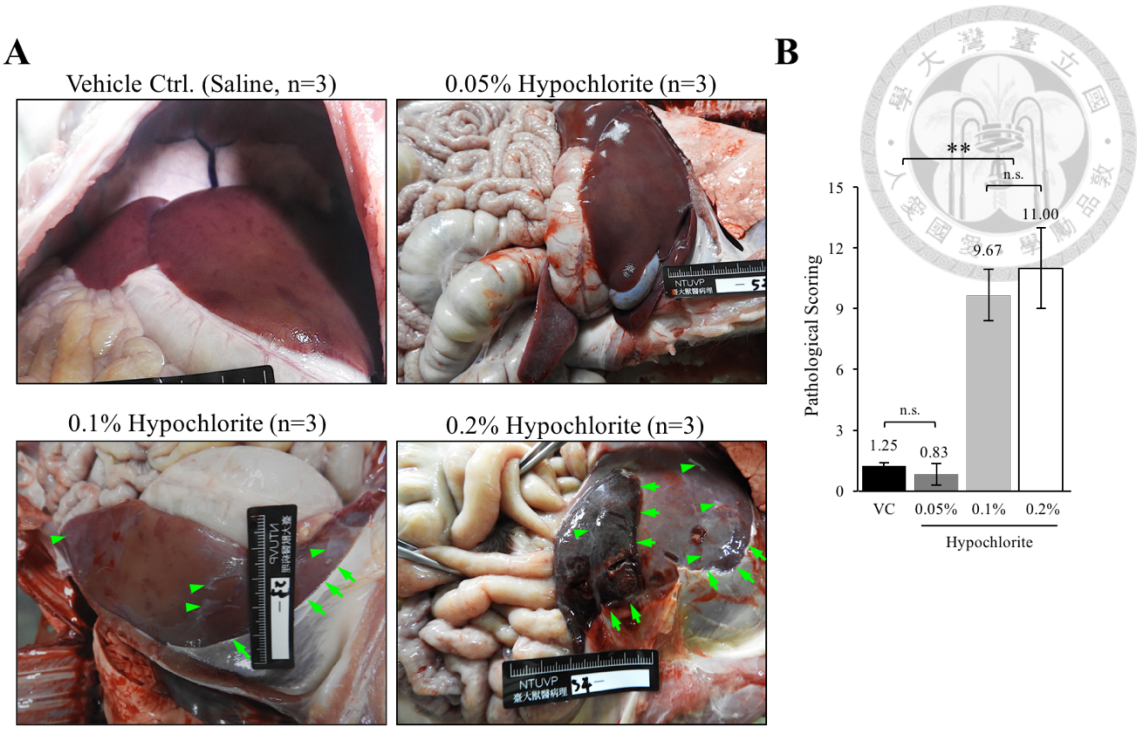


**Figure 9** Pathological necropsy examination showed dose-dependent severity of visceral organ fibrosis and adhesions

Necropsy was performed one week after the treatments. A. Gross findings of abdominal organs in pigs treated with different concentrations of SHC. Saline was used as vehicle control. Green arrows indicated adhesions between visceral organs or between abdominal wall with organs; green arrowheads indicated fibrotic appearance on the surface of the organs. B. Quantitative pathological evaluations by modified adhesion scoring system showed the lesions in 0.1 or 0.2 % SHC treated pigs were statistically more severe than saline- or 0.05% SHC-treated pigs. Representative images from 3 individual pigs of each group were presented.

### 3.2.2 Histological analyses demonstrated dose-dependent thickening and accumulation of collagen at the surface of visceral organs

To validate whether postmortem pathological examination of fibrotic appearance and thickening of tissues were due to collagen deposition, Masson's trichrome stain was carried out. As showed in figure 10, no to minimal amount of collagen signal was



doi:10.6342/NTU201903182

observed at the surface of abdominal wall (the single layer of the mesothelial cell was marked with arrow heads), liver, duodenum and omentum in control and 0.05% SHC-treated pigs (Fig. 10). In a sharp contrast, a dose-dependent thickening of collagen-containing fibrotic layer was observed in 0.1% and 0.2% SHC-treated pigs. Moreover, an increase number of spindle-shape cells were also observed in tissues obtained from 0.1% and 0.2% SHC-treated pigs (Fig. 10). Unexpectedly, unlike in liver, duodenum and omentum, we observed less collagen deposition at the surface of abdominal wall under 0.2% SHC stimulation; instead, a compact stack of spindle-shaped cells was accumulated above the layer of SM connective tissue (area below the dashed line) in the abdominal wall (Fig. 10). To further quantify the thickening of the tissues examined, an objective multipoint measurement on the surface thickening was performed as described in methods section. As showed in Fig. 11A, in contrast to a dose-dependent surface thickening measured in liver, 0.1% SHC resulted in the most significant surface thickening in ventral peritoneal wall and duodenum, and also resulted in the thickest surface thickening among other treatment groups. When collagen deposition analysis was further carried out, similar to the results in surface thickening analysis, 0.1% SHC resulted in the most significant collagen deposition in most of the organ examined (Fig. 11B), these data supported the fact that the observed and measured surface thickening of visceral organs under SHC treatments were resulted from collagen accumulation at



doi:10.6342/NTU201903182

the surface of these organs.

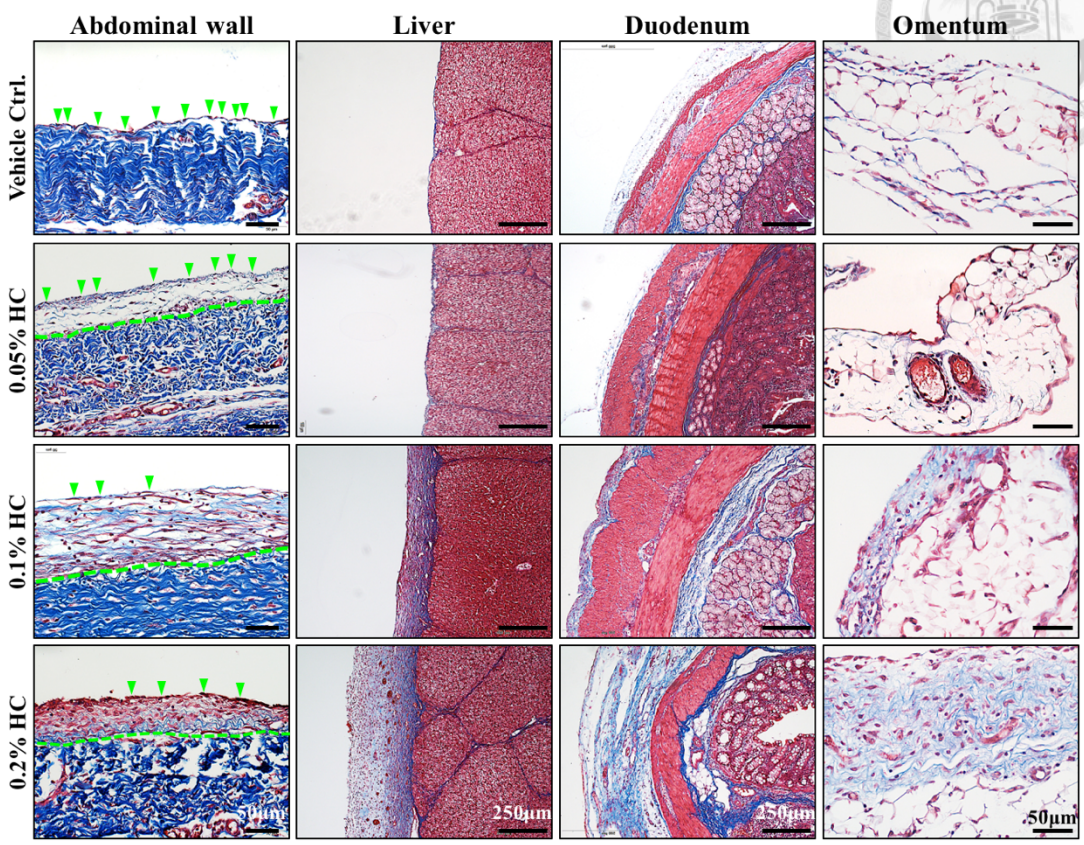


**Figure 10** Masson's Trichrome stain revealed a dose-dependent collagen deposition and thickening of tissue surface in SHC-treated pigs

A single lining of surface mesothelial cells (indicated with green arrow heads) was observed above the submesothelial connective tissue layer in ventral peritoneum of control pigs. However, a dose-dependent thickening of submesothelial compact zone was observed in SHC-treated piglets. Distance between the surface mesothelial cell layer (green arrowheads) and submesothelial connective tissue layer (underneath the green dash line) was marked. A dose-dependent thickening of surface capsule was also detected in the liver and the intestine (duodenum). Accumulation of collagen was detected in the omentum obtained from SHC-treated piglets. Representative images from 3 individual pigs of each group were presented.



doi:10.6342/NTU201903182

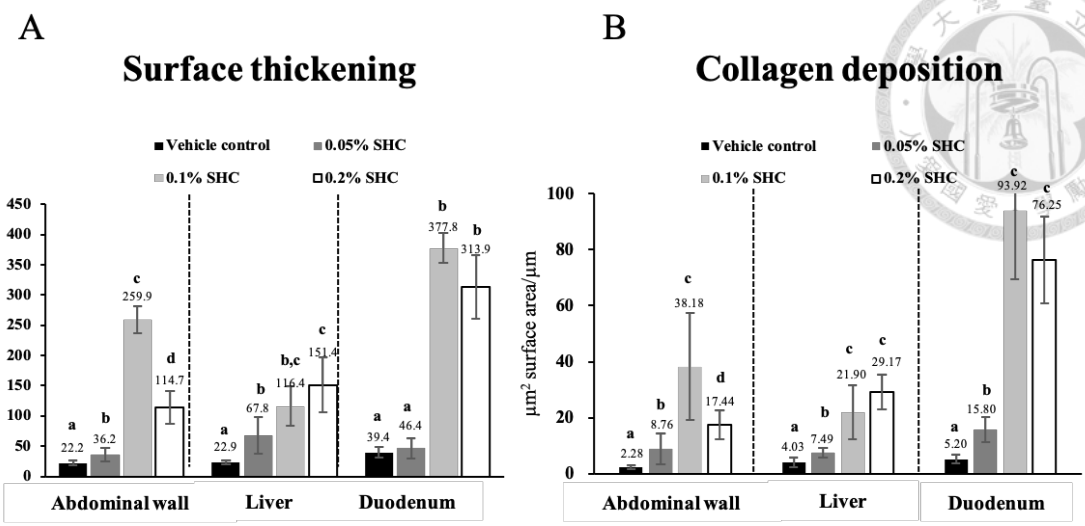


**Figure 11** Quantification analyses demonstrated a dose-dependent surface thickening and collagen accumulation in SHC-treated pigs

SHC-induced surface thickening (A) and collagen deposition (B) were quantified by CellSens Software. A dose-dependent thickening and collagen deposition was most apparent in liver, in both peritoneal wall and duodenum, 0.1% SHC stimulation exhibited higher degree of cell surface thickening and collagen accumulation than that of 0.2% SHC group. a-d indicate significant difference between groups. Statistical significance was set at $p<0.05$.

### 3.2.3 Immunofluorescent study demonstrated the loss of mesothelial cells and accumulation of α-smooth muscle actin positive myofibroblasts in SHC-treated pigs

Loss of mesothelial cells and increase accumulation of α-SMA+ myofibroblast at the SM compact zone are important characteristics of fibrotic peritoneal wall. To investigate the level of SHC-induced damages on peritoneum, immunofluorescent stains of mesothelial cell marker, cytokeratin (CK, in green) and myofibroblast marker, α-SMA (in red) were carried out. As showed in Fig. 12A, mesothelium labeled with CK was observed throughout the entire surface of peritoneum in control pigs with no



doi:10.6342/NTU201903182

accumulation of α-SMA+ myofibroblasts at the SM compact zone; however, when pigs were treated with SHC, different degrees of mesothelium fragmentation as well as α-SMA+ myofibroblasts accumulation were observed. Enlarged magnification images depicted the level of mesothelium integrity and the accumulations of α-SMA+ myofibroblasts under different SHC treatments (Fig. 12A, inset images). Accumulation of α-SMA+ myofibroblasts was observed not only at the surface, but also between all adherent junctions of visceral organs. As showed in Fig. 12B, these spindle-shaped α-SMA+ myofibroblasts were also positive and surrounded by collagen under Masson's trichrome stain indicating these myofibroblasts could be collagen producing cells as described in our earlier mouse model[5]. Three-dimensional reconstruction images of ventral peritoneum further confirmed and supported the integrity of peritoneal membrane in control pigs without the accumulation of α-SMA+ myofibroblasts at the SM compact zone (Fig. 12C, left panel). Loss of CK+ mesothelial cells with an increase accumulation of α-SMA+ myofibroblasts underneath the remaining mesothelial cells was apparent in SHC-treated pigs (0.1% SHC group was used as an example in Fig. 12C, right panel).



doi:10.6342/NTU201903182

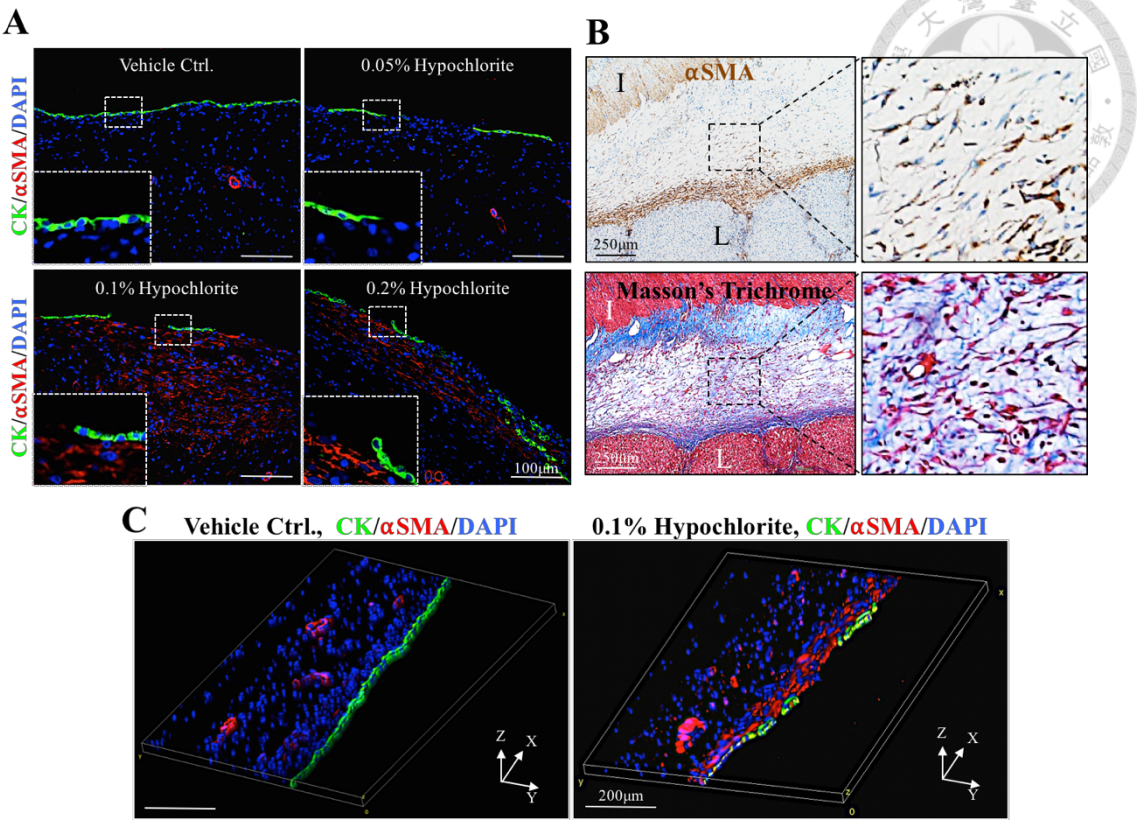


**Figure 12** Indirect immunofluorescent stain showed mesothelium fragmentation and accumulation of α smooth muscle actin positive (αSMA+) cells in SHC-treated pigs (A) SHC-induced fragmentation of mesothelium of ventral abdominal wall (labeled with cytokeratin in green) and accumulation of αSMA+ cells (labeled in red) at the submesothelial region of ventral abdominal wall. Higher magnification showed continuation of cytokeratin positive mesothelial cells with minimal amount of αSMA+ cells in control pig, and discontinued mesothelium with αSMA+ cells in SHC-treated groups. (B) Histochemistry and Masson's Trichrome studies demonstrated spindle-shape αSMA+ cells (upper panels) accumulated at the adherent junction between two visceral organs and were surrounded with intense deposited collagen (lower panels). I: intestine, L: liver (C) 3D reconstruction images confirmed the integrity of mesothelium in control pigs and the accumulation of αSMA+ cells at the submesothelial region of the abdominal wall. Representative images from 3 individual pigs of each group were presented.

Quantification analyses further confirmed a reciprocally, but dose-dependent level of remaining mesothelial cells at the surface of ventral peritoneum. When compared with control pigs which displayed a relatively intact mesothelium (90.7±5.5% of the



doi:10.6342/NTU201903182

remaining mesothelial cells), pigs treated with 0.05% and 0.1% SHC exhibited 66.5±11.8% and 49.5±8.3% of the remaining mesothelial cells at the surface of peritoneal wall (Fig. 13A). In a sharp contrast, pigs treated with 0.2% SHC, a significant decrease of CK+ signal was measured (30.7±6.6%) (Fig. 13A). When α-SMA+ myofibroblasts was further quantified, we observed a significant increase of α-SMA+ myofibroblasts in 0.1% SHC-treated group (57.95%, Fig. 13B), although minimal signals of α-SMA+ myofibroblasts were also observed at the SM region in 0.2% SHC group, but quantification analysis indicated no statistical difference when compared with control and 0.05% groups (Fig. 13B, 0.55%, 2.26% and 2.54% for control, 0.05% SHC and 0.2% SHC group, respectively).

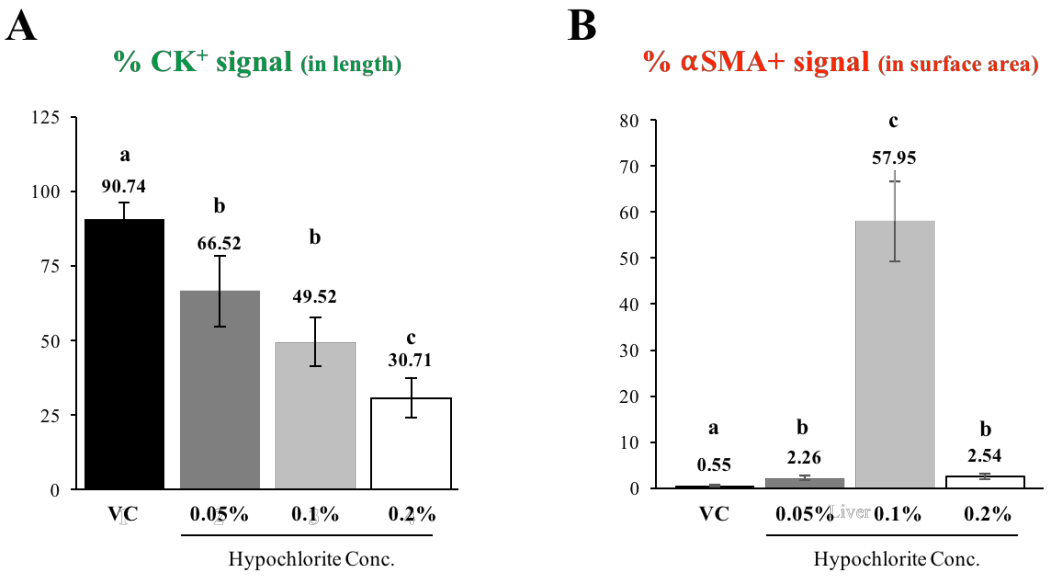


**Figure 13** Quantification analyses showed mesothelium fragmentation and accumulation of α smooth muscle actin positive cells in SHC-treated pigs
Quantification analyses showed a dose-dependent loss of mesothelium (A) under SHC treatments. However, a significant accumulation of αSMA+ cells was only observed in 0.1%, but not in 0.2% SHC-treated group (B). a-d indicate significant



doi:10.6342/NTU201903182

difference between groups. Statistical significance was set at $p<0.05$.

## 3.3 Cytokine

### 3.3.1 Inflammatory cytokines IL1-β, TNF-α and TGF-β1 were elevated in SHC-treated pigs.

In end point model, inflammatory cytokine IL1-β, TNF-α were measured in serum samples via ELISA whereas changes of TGF-β1 gene expression in abdominal wall tissue sample was carried out with real-time PCR. As showed in Fig. 14, IL1-β level was elevated in all three SHC-treated groups (1.51±0.10, 1.36±0.20 and 1.11±0.08) times more in 0.05%, 0.1% and 0.2%, respectively than its own pretreat condition) (Fig. 14A). As for TNF-α, significant elevation was only detected in 0.05% group (1.51±0.12 times more than pretreat) (Fig.14B). However, serum TGF-β1 was below the detection limit of ELISA used in this study (data not shown); therefor, real-time PCR was further carried out to examine the changes of TGF-β1 gene expression. As showed in Fig. 14C, besides 0.05% group exhibited significant up regulation in TGF-β1 gene expression, no other differences were detected (Fig. 14C).



doi:10.6342/NTU201903182

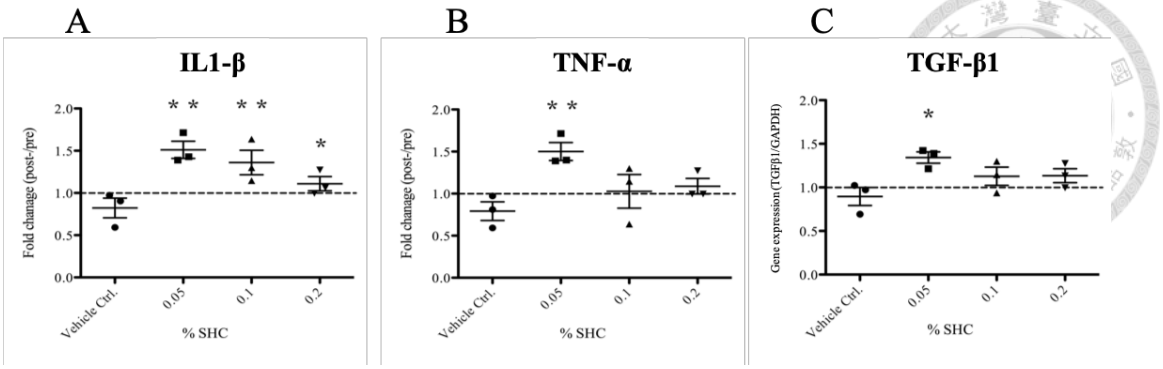


**Figure 14** ELISA and real-time PCR showed elevated inflammatory cytokines in 0.05% and 0.1% SHC-treated groups
**P<0.01, *P<0.05

### 3.3.2 Cytokine measurements from abdominal lavage showed higher IL1-β and TNF-α in 0.1% SHC-treated pigs at day 2.

In order to evaluate whether cytokine secretion within the peritoneal cavity can be measured and whether this measurement can represent better the local inflammation of peritoneal cavity and visceral organs, abdominal lavage was collected and used for ELISA. As showed in Fig. 15, an elevation of IL1-β (2.8±0.81 fold) and TNF-α (4.2±1.67 fold) was measured from day 2 post 0.1% SHC treatment. Although a trend in IL1-β and TNF-α was observed, but these changes did not reach statistic difference. After activation of TGF-β1 in the concentrated lavage, TGF-β1 showed a slightly decrease of TGF-β1 in day 2 post-hypochlorite treatment followed by a significantly increase in day 4 samples when compared with day -5 (starting point) (Fig. 15).



doi:10.6342/NTU201903182

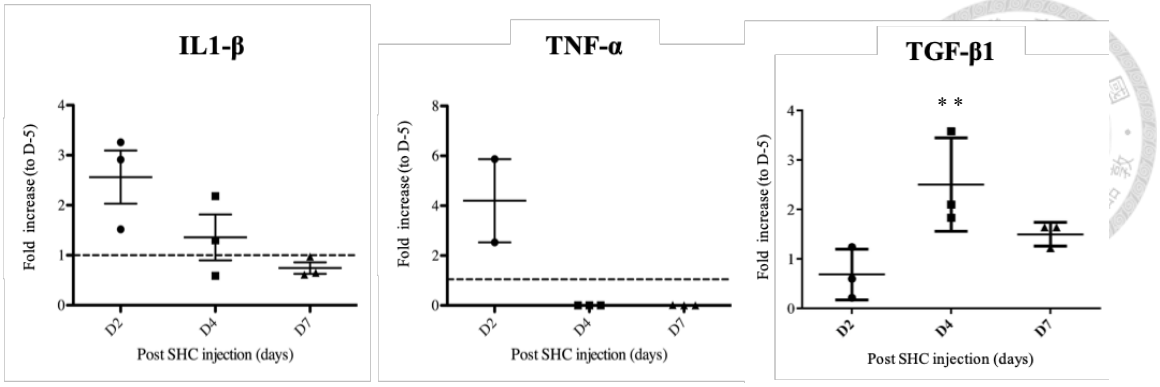


**Figure 15** Concentrated lavage samples revealed elevation of IL1-β and TNF-α after 0.1% SHC treatment at day 2 and gradually fall back to normal after day 4. TGF-β1 concentrations showed > two times increase at day 4 post-hypochlorite treatment.

### 3.3.3 Immunofluorescent study demonstrated increase of TGF-β1 expressing cells in SHC-treated pigs

Although TGF-β1 can not be detected in either serum or lavage samples without activation, immunofluorescent study showed increase protein expression in SHC-treated pigs. In control pigs, no TGF-β1 signal was detected besides on the endothelium and parenchyma of the liver (Fig. 16 in green). On the other hand, mesothelium labeled with CK was observed throughout the entire surface of peritoneum, liver and duodenum in control pigs (Fig. 16 in red). However, after treated with 0.1% SHC, TGF-β1 was detected in submesothelial compact zone in the abdominal wall and in cells at the surface of liver and duodenum. This is more apparent in day 4-7 that TGF-β1 signal was highly expressed in lining cells of abdominal wall (Fig. 16 in green, insets). Unlike in abdominal wall, TGF-β1 was observed accumulated within the thickened tissue surface in liver and duodenum. Some remanding mesothelial cells ($CK^+$ cells) showed



doi:10.6342/NTU201903182

TGF-β1 signal in day 4-7 (Fig. 16).

### 3.3.4 Immunofluorescent study demonstrated an increase of CX3CL1 expressing cells in SHC-treated pig

The chemokine CX3CL1 (fractalkine), has been detected in endothelium, epithelium, fibroblasts, human peritoneal cells and in the peritoneal cavity of mice during bacterial peritonitis [22]. Helmke et al. have demonstrated that IL-1β promotes CX3CL1 expression on mesothelium and enhances TGF-β, which subsequently promote PD associated fibrosis[18]. In order to investigate whether SHC-induced PF share the similar pathogenesis as observed in PD patients, CX3CL immunostaining was carried out in tissues of SHC-treated pigs. Here we demonstrated that in control pigs, weak CX3CL1 signal was detected above submesothelial compact zone and parenchyma of liver. In contrast, the expression of CX3CL1 was elevated in 0.1% SHC-treated pigs. Moreover, strong signals were detected on the remaining mesothelial cells as part of the $CX3CL1^+$ cells were also $CK^+$. (Fig. 17).



doi:10.6342/NTU201903182

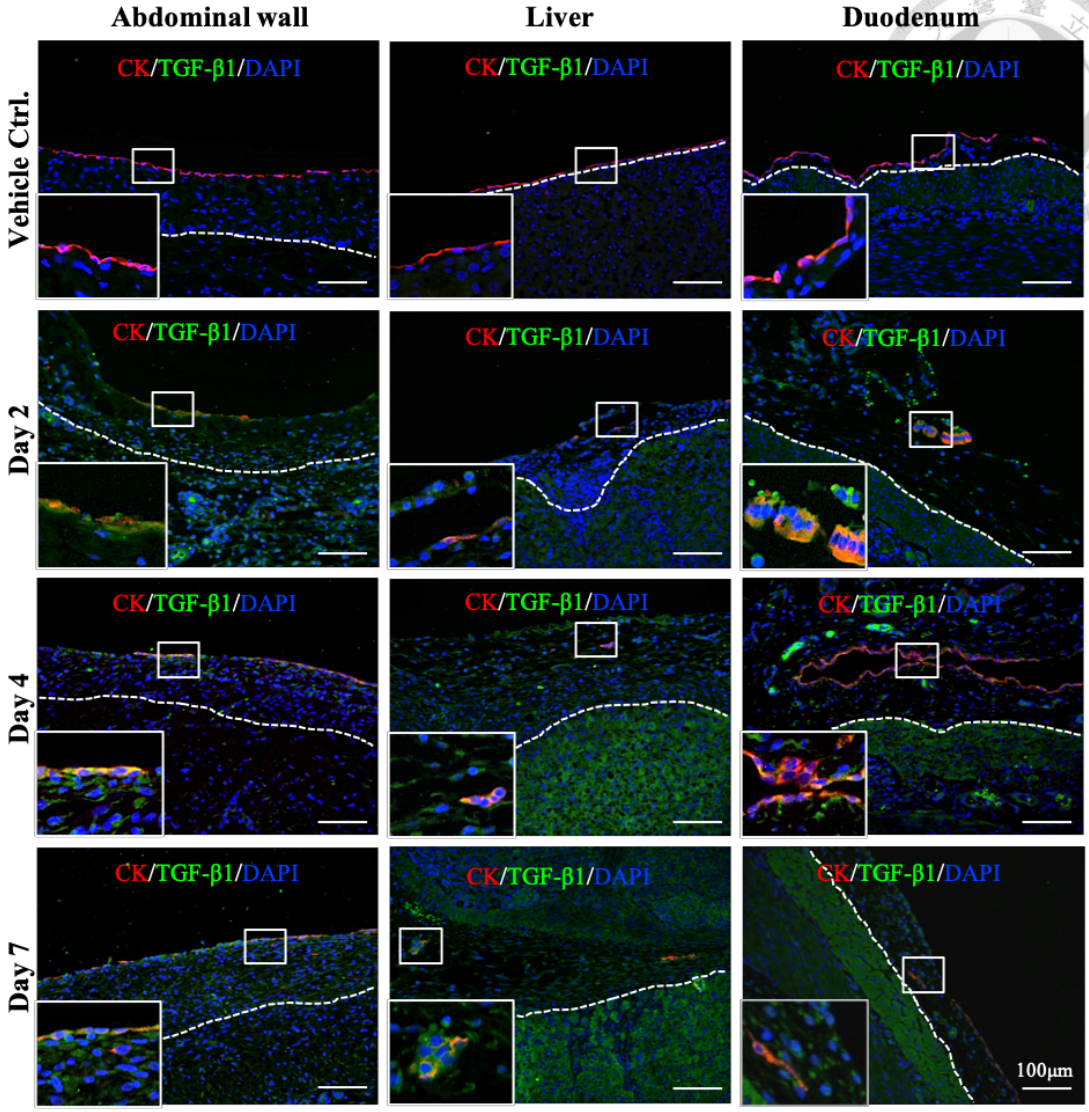


**Figure 16** Immunofluorescent study revealed TGF-β1 expression on the tissue surface in SHC-treated pigs

A lining of cells above submesothelial connective tissue layer showed no signal of TGF-β1 in control pigs. However, after 0.1% SHC injection, TGF-β1 positive cells was shown in submesothelial compact zone of abdominal wall (day 2, 4, 7). Strong TGF-β1 signal was observed at the mesothelium after day 4. In liver and duodenum, TGF-β1 accumulated along with the thickening of the tissue surface. Remaining MCs also showed TGF-β1 signals. White dash lines refer to submesothelial connective tissue layer in abdominal wall and parenchyma in liver/duodenum, respectively.



doi:10.6342/NTU201903182

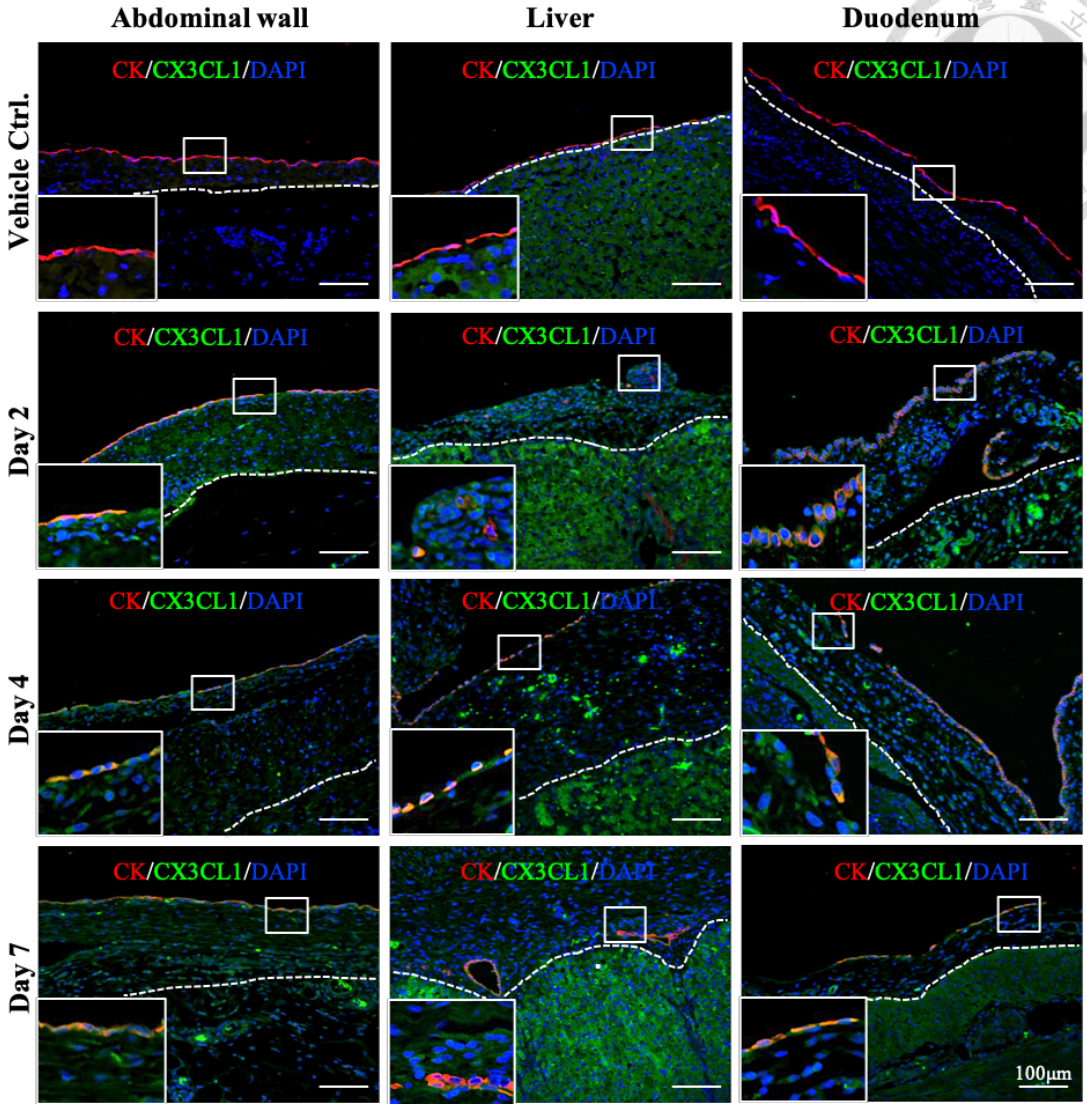


**Figure 17** Immunofluorescent study revealed CX3CL1 expression at the tissue surface in SHC-treated pigs

In control pigs, no CX3CL1 signal was detected from the mesothelium. In contrast, the expression of CX3CL1 was elevated in 0.1% SHC-treated pigs. Most of the signals were detected at the surface of lining cells (mesothelial cells), but in day2 abdominal wall, day4 liver and day4 duodenum, CX3CL1 was also expressed in submesothelial compact zone and the thickened tissue surface. Remaining MCs also showed CX3CL1 signals. White dash lines refer to submesothelial connective tissue layer in abdominal wall and parenchyma in liver/duodenum respectively.



doi:10.6342/NTU201903182

**Figure 18** QR code link for supplementary Video 1-4 Laparoscopy examination of peritoneal cavity
Supplementary Video 1-4 refers to control, 0.05%, 0.1%, 0.2% SHC treated pig (1 week after injection). Representative video was presented.
https://drive.google.com/drive/folders/1NhPKkS-KUP34ytIHDSJG_9yKFDVgoMEY?usp=sharing



doi:10.6342/NTU201903182

# Chapter 4 Discussions

Peritoneal fibrosis (PF) resulted from PD or peritoneal injury often hampers the efficiency of PD and normal function of visceral organs. Despite mechanisms and pathogenesis of fibrosis have been studied for decades, prevention and treatments of PF are still in progress[52,53,55]. For patients who undergo PD and develop simple sclerosis or EPS, innovated, effective and safe therapies to prevent PF is urgently needed. In this thesis, we established for the first time, porcine model of PF and visceral organ adhesions and provide comprehensive evaluation methods for not only validating findings from murine models and but also explore its potentials on future evaluation on the feasibility, efficiency and clinical safety of therapeutic treatments.

We observed unlike in mouse which 0.05% SHC (0.05mM in 1-1.5ml volume) could already cause PF[5], we demonstrated in pigs that fibrosis and surface thickening of ventral peritoneum as well as visceral organs occurred only after 0.1%- 0.2% (0.1-0.2 mM) SHC administration. Moreover, adhesions between intestines or liver lobes were observed only in higher SHC concentrations of 0.1% and 0.2%, and not under 0.05% SHC stimulation as described earlier in rodent species[5,27]. Nevertheless, in agreement with observations in mouse, we showed in our pig model, a dose-dependent increase of surface collagen accumulation, fragmentation and loss of ventral peritoneum mesothelial cells and accumulation of α-SMA$^{+}$ myofibroblasts at the SM



doi:10.6342/NTU201903182

region in SHC-treated pigs. Our data demonstrated that animal model of PF can be established in pig and both ante- and postmortem analyses established in current study could be carried out in pig model to access the degree of peritoneal injury and fibrosis. Pathological findings in current pig model are comparable with data obtained from mouse model of earlier study[5], apparent collagen deposition was observed at the surface of visceral organs and between two adhered organs after 0.1% and 0.2% SHC treatment. Earlier studies in mouse used lineage tracing technique demonstrated that the main source of peritoneal myofibroblasts is SM fibroblasts instead of mesothelial cells undergo EMT process[5]. The major difference between mesothelial cell, myofibroblasts and matured fibroblast is the presence of protein marker of α-SMA. With immunohistochemistry study using myofibroblasts specific marker α-SMA, we showed the presence and the accumulation of α-SMA$^+$ myofibroblasts at the SM layer and at the adhered junction of visceral organs. From immunofluorescent study, we also showed that under 0.1% SHC treatment, the presence and the accumulation of α-SMA at the SM compact zone was most apparent among different dosages of SHC tested. The less amount of α-SMA$^+$ cells detected in 0.2% SHC group likely due to the transition of myofibroblasts (α-SMA$^+$) to matured fibroblast (α-SMA$^-$) upon the progression of PF.

Current study aim to establish porcine model of PF for future evaluation of therapeutic



doi:10.6342/NTU201903182

options (e.g. cell therapy) and inhibition of PF. Based on results from this thesis, we considered 0.1% SHC is a suitable dosage for creating PF in pig for the purpose of above-mentioned treatment assessments. Although 0.05% SHC did resulted in minor collagen deposition and surface thickening on liver, and caused the loss of mesothelial cells on ventral peritoneum; however, the degree of damages and pathological changes were minor. On the other hand, under 0.2% SHC stimulation, despite severe fibrosis and adhesions of visceral organs were observed, pronounced thickening of visceral organs and collagen deposition were also measured; however, under this SHC concentration, only 30.7% of the mesothelium was remained on the ventral peritoneum. It is known that denudation of peritoneal mesothelial cells happens after injury, and mesothelium can be partially repaired by surviving mesothelial cells under the stimulation of injected cells from the cell therapy[5,29,36], thus, the number of remaining mesothelial cells would affect the efficacy and the outcome of therapeutic treatments tested. At 0.1% SHC, all pigs exhibited consistent gross pathological changes under necropsy examination, in addition, significant increase of surface thickness and collagen deposition were measured in all organs examined, more importantly, despite apparent pathological damages were observed, in contrast to 0.2% SHC group only 30.7% of the remaining mesothelial cells, in 0.1% SHC group, about half (49.5%) of the mesothelial cells could still be detected at the surface of ventral



doi:10.6342/NTU201903182

peritoneum with considerable amount of α-SMA$^+$ myofibroblast accumulated at the SM compact zone. Based on all above-mentioned characteristics and measurements carried out in current study, we consider 0.1% SHC induced a moderate to severe pathological status in pig and is suitable for the study of cell therapy (for the repair or regeneration of mesothelium) and inhibition of fibrosis process (for the reduction of α-SMA$^+$ myofibroblast accumulation).

To further investigate the progression of SHC-induced peritoneal fibrosis, we therefore chose 0.1% SHC as the stimulation concentration for time course progression model base on the reasons mentioned above. In this model, besides regular serum collection, we also conducted peritoneal lavage to examine the changes at local (peritoneal cavity) environment. Unlike lavage samples obtain from rodent species which can directly be used for ELISA analysis[28], lavage sample obtained from pigs has to be concentrated before any evaluation due to its larger volume. However, we observed that even after 10 times concentration, the amount of TGF-β1 was still below the detection limit (2 pg/ml) of our ELISA kit without pre-activation of the samples. To overcome this problem, a higher concentration rate or lower amount of infused saline may help to improve this situation. On the other hand, after activation of pre-existing latent form of TGF-β1, the activated TGF-β1 was increase at day 4-7. Compare to day-5, day 2 was slightly decrease, this may because TGF-β1 was used after SHC insult. In order to



doi:10.6342/NTU201903182

compromise the consumption, more TGF-β1 was made and be detected in lavage samples in day 4 and 7.

In PD patients, various stimuli within dialysate promote MCs and macrophages to produce proinflammation cytokines and growth factors like TNF-α, IL-1β, IL-6, VEGF and TGF-β1. Constant stimulation by these cytokine and growth factors lead to chronic inflammation and angiogenesis in the peritoneal cavity[40]. These processes promote the recruitment of resident fibroblast and collagen synthesis at the injury site, which result in PF. In fact, the mechanisms of SHC-induced PF have not been reported yet. In this thesis, we investigated the pathogenesis of SHC-induced and PD related PF. Serum IL1-β, TNF-α and TGF-β1 were elevated at 7 days after 0.05% SHC-treated pigs compare to control pigs (Fig. 14). IL1-β and TNF-α in lavage sample also showed upward trend at 2 days after 0.1% SHC treatment (Fig. 15). Immunofluorescent study revealed a TGF-β1 deposition at the tissue surface in 0.1% SHC-treated pigs (Fig. 16). These data indicate that SHC induces the secretion of inflammation cytokine, likely via the stimulation of MCs and macrophage which is similar to the initial pathogenesis of PD. Recent study reported that PD fluid induces macrophage to secret IL-1β, which promotes CX3CL1 expression in MCs. The interaction of the stalked chemokine CX3CL1 on peritoneal mesothelium with its receptor CX3CR1 on macrophages promoted chronic inflammation and fibrosis in a peritoneal dialysis mouse



doi:10.6342/NTU201903182

model[18].To correlate SHC-induced PF to PD related PF, we also examine the expression of CX3CL1 in SHC-induced pig model. In this present study, we demonstrated that the CX3CL1 signal was increased on the lining cell on abdominal wall, liver and duodenum in 0.1% SHC treated pigs (Fig. 17). The remaining MCs showed both TGF-β1 and CX3CL1 signal, this match with the reported study that MCs can secret these cytokines that participate the progression of PF. Moreover, some cells observed at submesothelial compact zone also showed positive signal of CX3CL1, which might be the macrophage. Further studies on the identification of those CX3CL1 positive cells present in our SHC model is required for the understanding on the pathogenesis of SHC-induced peritoneal fibrosis.



doi:10.6342/NTU201903182

# Chapter 5 Conclusions and future work

Taken together, our study demonstrated for the first time that pig is useful for establishing animal model of PF at 0.1% (0.1mM) dosage. Antemortem ultrasoungraphy and laparoscopy examination provide instant feedback on the progression of PF and is suitable for evaluating the efficacy of treatments at any time point without sacrificing the animals. To our knowledge, these antemortem evaluations have never been performed in other animal species, and are certainly difficult to execute in rodent species. Combine postmortem histology, marker protein assessments (cytokeratin for mesothelial cells, α-SMA for myofibroblast) and quantification; detail analyses could further be performed to generate useful information about the potential of treatments. The underlying mechanism of SHC-induced PF likely share similar pathogenesis with PD-induced PF as we showed in time course progression experiment, acute inflammatory cytokine, IL-1β, TNF-α, TGF-β1 exhibited upward trend in 0.1% SHC-treated pigs, and increase expression of chemokine CX3CL1 at the lining of tissue surface and within the thickened submesothlium compact zone support the similarities of SHC-induced fibrosis with PD-induced fibrosis.

In conclusion, PF is a complex process; unfortunately, no current animal model shares high physiological and anatomical similarities with human, therefore, this study using pig may provide an alternative and more suitable animal model for the study human PF



doi:10.6342/NTU201903182

and intra-abdominal organ adhesions. This model can also be used to evaluate the efficacy of potential candidates on the prevention (e.g. compounds) and treatments (e.g. stem cells) for regenerative medicine.



doi:10.6342/NTU201903182

# References

1. NephCure Kidney International https://nephcure.org/peritoneal-dialysis/.
2. TeachMeAnatomy https://teachmeanatomy.info/abdomen/areas/peritoneum/.
3. Abelardo Aguilera MaYne-M, Rafael Selgas, Francisco Sánchez-Madrid,, and López-Cabrera M. Epithelial to mesenchymal transition as a triggering factor of peritoneal membrane fibrosis and angiogenesis in peritoneal dialysis patients. Current Opinion in Investigational Drugs 6: 2005.
4. Blitek A, Kaczmarek MM, Kiewisz J, and Ziecik AJ. Endometrial and conceptus expression of HoxA10, transforming growth factor beta1, leukemia inhibitory factor, and prostaglandin H synthase-2 in early pregnant pigs with gonadotropin-induced estrus. Domest Anim Endocrinol 38: 222-234, 2010.
5. Chen YT, Chang YT, Pan SY, Chou YH, Chang FC, Yeh PY, Liu YH, Chiang WC, Chen YM, Wu KD, Tsai TJ, Duffield JS, and Lin SL. Lineage tracing reveals distinctive fates for mesothelial cells and submesothelial fibroblasts during peritoneal injury. Journal of the American Society of Nephrology : JASN 25: 2847-2858, 2014.
6. Cho YJ, Lee YA, Lee JW, Kim JI, and Han JS. Kinetics of proinflammatory cytokines after intraperitoneal injection of tribromoethanol and a tribromoethanol/xylazine combination in ICR mice. Lab Anim Res 27: 197-203, 2011.
7. Coester AM, Smit W, Struijk DG, and Krediet RT. Peritoneal function in clinical practice: the importance of follow-up and its measurement in patients. Recommendations for patient information and measurement of peritoneal function. NDT Plus 2: 104-110, 2009.
8. Danford CJ, Lin SC, Smith MP, and Wolf JL. Encapsulating peritoneal sclerosis. World J Gastroenterol 24: 3101-3111, 2018.
9. Dawson HD, Smith AD, Chen C, and Urban JF, Jr. An in-depth comparison of the porcine, murine and human inflammasomes; lessons from the porcine genome and transcriptome. Vet Microbiol 202: 2-15, 2017.
10. Del Peso G, Jimenez-Heffernan JA, Bajo MA, Aroeira LS, Aguilera A, Fernandez-Perpen A, Cirugeda A, Castro MJ, de Gracia R, Sanchez-Villanueva R, Sanchez-Tomero JA, Lopez-Cabrera M, and Selgas R.



doi:10.6342/NTU201903182

Epithelial-to-mesenchymal transition of mesothelial cells is an early event during peritoneal dialysis and is associated with high peritoneal transport. Kidney Int Suppl S26-33, 2008.
11. do Amaral R, Arcanjo KD, El-Cheikh MC, and de Oliveira FL. The Peritoneum: Health, Disease, and Perspectives regarding Tissue Engineering and Cell Therapies. Cells Tissues Organs 204: 211-217, 2017.
12. Dyson MC, Alloosh M, Vuchetich JP, Mokelke EA, and M. S. Components of Metabolic Syndrome and Coronary Artery Disease in Female Ossabaw Swine Fed Excess Atherogenic Diet. Comparative Medicine 56: 35-45, 2006.
13. Fang CC, Huang JW, Shyu RS, Yen CJ, Shiao CH, Chiang CK, Hu RH, and Tsai TJ. Fibrin-Induced epithelial-to-mesenchymal transition of peritoneal mesothelial cells as a mechanism of peritoneal fibrosis: effects of pentoxifylline. PLoS One 7: e44765, 2012.
14. Ghellai AM, Stucchi AF, Chegini N, Ma C, Andry CD, Kaseta JM, Burns JW, Skinner KC, and JM. B. Role of transforming growth factor beta-l in peritonitis-induced adhesions. J Gastrointest Surg 4: 316-323, 2000.
15. Gotloib L, Crassweller P, Rodella H, Oreopoulos DG, Zellerman G, Ogilvie R, Husdan H, Brandes L, and S. V. Experimental Model for Studies of Continuous Peritoneal'Dialysis in Uremic Rabbits. Nephron 31: 254-259, 1982.
16. Gyöngyösi M, Pavo N, Lukovic D, Zlabinger K, Spannbauer A, Traxler D, Goliasch G, Mandic L, Bergler-Klein J, Gugerell A, Jakab A, Szankai Z, Toth L, Garamvölgyi R, Maurer G, Jaisser F, Zannad F, Thum T, Bátkai S, and Winkler J. Porcine model of progressive cardiac hypertrophy and fibrosis with secondary postcapillary pulmonary hypertension. Journal of Translational Medicine 15: 2017.
17. Heimbürger O, Waniewski J, Warynski A, Tranæus A, and Lindholm B. Peritoneal transport in CAPD patients with permanent loss of ultrafiltration capacity. Kidney International 38: 495-506, 1990.
18. Helmke A, Nordlohne J, Balzer MS, Dong L, Rong S, Hiss M, Shushakova N, Haller H, and von Vietinghoff S. CX3CL1-CX3CR1 interaction mediates macrophage-mesothelial cross talk and promotes peritoneal fibrosis. Kidney Int 95: 1405-1417, 2019.
19. Huang JW, Yen CJ, Wu HY, Chiang CK, Cheng HT, Lien YC, Hung KY, and Tsai TJ. Tamoxifen downregulates connective tissue growth



doi:10.6342/NTU201903182

factor to ameliorate peritoneal fibrosis. Blood Purif 31: 252-258, 2011.
20. Hung KY, Shyu RS, Fang CC, Tsai CC, Lee PH, Tsai TJ, and Hsieh BS. Dipyridamole inhibits human peritoneal mesothelial cell proliferation in vitro and attenuates rat peritoneal fibrosis in vivo. Kidney Int 59: 2316-2324, 2001.
21. Io H, Hamada C, Ro Y, Ito Y, Hirahara I, and Tomino Y. Morphologic changes of peritoneum and expression of VEGF in encapsulated peritoneal sclerosis rat models. Kidney Int 65: 1927-1936, 2004.
22. Ishida Y, Hayashi T, Goto T, Kimura A, Akimoto S, Mukaida N, and Kondo T. Essential involvement of CX3CR1-mediated signals in the bactericidal host defense during septic peritonitis. J Immunol 181: 4208-4218, 2008.
23. Judge EP, Hughes JM, Egan JJ, Maguire M, Molloy EL, and O'Dea S. Anatomy and bronchoscopy of the porcine lung. A model for translational respiratory medicine. Am J Respir Cell Mol Biol 51: 334-343, 2014.
24. Junor BJ, Briggs D, Forwell MA, Dobbie JW, and I. H. Sclerosing peritonitis—the contribution of chlorhexidine in alcohol. . Peritoneal dialysis international : journal of the International Society for Peritoneal Dialysis 5: 4, 1985.
25. Kemter E, and Wolf E. Pigs pave a way to de novo formation of functional human kidneys. Proc Natl Acad Sci U S A 112: 12905-12906, 2015.
26. Lai KN, Lai KB, Lam CW, Chan TM, Li FK, and JC. L. Cytokine profiles in peritoneal dialysis effluent predicts the peritoneal solute transport rate in continuous ambulatory peritoneal dialysis patients. Am J Kidney Dis 35: 644-652, 2000.
27. Levine S, and A. S. Abdominal cocoon: An animal model for a complication of peritoneal dialysis. Peritoneal dialysis international : journal of the International Society for Peritoneal Dialysis 16: 613-616, 1996.
28. Li J, Zhang Y, Lou J, Zhu J, He M, Deng X, and Cai Z. Neutralisation of peritoneal IL-17A markedly improves the prognosis of severe septic mice by decreasing neutrophil infiltration and proinflammatory cytokines. PLoS One 7: e46506, 2012.
29. Lua I, Li Y, Pappoe LS, and Asahina K. Myofibroblastic Conversion and Regeneration of Mesothelial Cells in Peritoneal and Liver Fibrosis. Am J Pathol 185: 3258-3273, 2015.



doi:10.6342/NTU201903182

30. Mackow RC, Argy WP, Winchester JF, Rakowski TA, Fields PA, Rotellar C, and GE. S. Sclerosing encapsulating peritonitis in rats induced by long-term intraperitoneal administration of antiseptics. J Lab Clin Med 112(3): 363-371, 1988.
31. Mackow RC, Winchester JF, Argy WP, Andrews PM, Fields PA, Bates S, Rakowski TA, and GE. S. Sclerosing encapsulating peritonitis in rats: an experimental study with intraperitoneal antiseptics. Contributions to nephrology 57: 213-218, 1987.
32. Margetts PJ, Bonniaud P, Liu L, Hoff CM, Holmes CJ, West-Mays JA, and Kelly MM. Transient overexpression of TGF-{beta}1 induces epithelial mesenchymal transition in the rodent peritoneum. Journal of the American Society of Nephrology : JASN 16: 425-436, 2005.
33. Margetts PJ, Hoff C, Liu L, Korstanje R, Walkin L, Summers A, Herrick S, and Brenchley P. Transforming growth factor beta-induced peritoneal fibrosis is mouse strain dependent. Nephrology, dialysis, transplantation : official publication of the European Dialysis and Transplant Association - European Renal Association 28: 2015-2027, 2013.
34. Meng XM, Nikolic-Paterson DJ, and Lan HY. TGF-beta: the master regulator of fibrosis. Nat Rev Nephrol 12: 325-338, 2016.
35. Moinuddin Z, Summers A, Van Dellen D, Augustine T, and Herrick SE. Encapsulating peritoneal sclerosis-a rare but devastating peritoneal disease. Front Physiol 5: 470, 2014.
36. Mutsaers SE, Prele CM, Pengelly S, and Herrick SE. Mesothelial cells and peritoneal homeostasis. Fertil Steril 106: 1018-1024, 2016.
37. Nakamoto H, Imai H, Ishida Y, Yamanouchi Y, Inoue T, Okada H, and H. S. New animal models for encapsulating peri- toneal sclerosis—role of acidic solution. Peritoneal dialysis international : journal of the International Society for Peritoneal Dialysis 21: S349-353, 2001.
38. Noel JM, Fernandez de Castro JP, Demarco PJ, Jr., Franco LM, Wang W, Vukmanic EV, Peng X, Sandell JH, Scott PA, Kaplan HJ, and McCall MA. Iodoacetic acid, but not sodium iodate, creates an inducible swine model of photoreceptor damage. Exp Eye Res 97: 137-147, 2012.
39. Oliveira LG, Luengo J, Caramori JC, Montelli AC, Cunha Mde L, and Barretti P. Peritonitis in recent years: clinical findings and predictors of treatment response of 170 episodes at a single Brazilian center. Int Urol Nephrol 44: 1529-1537, 2012.
40. Onishi A. The Mechanism of Peritoneal Fibrosis in Peritoneal



doi:10.6342/NTU201903182

Dialysis. Journal of Nephrology & Therapeutics 01: 2012.
41. Pannekeet MM, Imholz ALT, Struijk DG, Koomen GCM, Langedijk MJ, Schouten N, de Waart R, Hiralall J, and Krediet RT. The standard peritoneal permeability analysis: A tool for the assessment of peritoneal permeability characteristics in CAPD patients. Kidney International 48: 866-875, 1995.
42. Sanderson N, Factor V, Nagy P, Kopp J, Kondaiah P, Wakefield L, Roberts AB, Sporn MB, and SS. T. Hepatic expression of mature transforming growth factor β 1 in transgenic mice results in multiple tissue lesions. Proc Natl Acad Sci U S A 92: 2572-2576, 1995.
43. Schwenger V, Morath C, Salava A, Amann K, Seregin Y, Deppisch R, Ritz E, Bierhaus A, Nawroth PP, and Zeier M. Damage to the peritoneal membrane by glucose degradation products is mediated by the receptor for advanced glycation end-products. Journal of the American Society of Nephrology : JASN 17: 199-207, 2006.
44. Seaton M, Hocking A, and Gibran NS. Porcine models of cutaneous wound healing. ILAR J 56: 127-138, 2015.
45. Seok J, Warren HS, Cuenca AG, Mindrinos MN, Baker HV, Xu W, Richards DR, McDonald-Smith GP, Gao H, Hennessy L, Finnerty CC, Lopez CM, Honari S, Moore EE, Minei JP, Cuschieri J, Bankey PE, Johnson JL, Sperry J, Nathens AB, Billiar TR, West MA, Jeschke MG, Klein MB, Gamelli RL, Gibran NS, Brownstein BH, Miller-Graziano C, Calvano SE, Mason PH, Cobb JP, Rahme LG, Lowry SF, Maier RV, Moldawer LL, Herndon DN, Davis RW, Xiao W, Tompkins RG, Inflammation, and Host Response to Injury LSCRP. Genomic responses in mouse models poorly mimic human inflammatory diseases. Proc Natl Acad Sci U S A 110: 3507-3512, 2013.
46. Su X, Zhou G, Wang Y, Yang X, Li L, Yu R, and Li D. The PPARbeta/delta agonist GW501516 attenuates peritonitis in peritoneal fibrosis via inhibition of TAK1-NFkappaB pathway in rats. Inflammation 37: 729-737, 2014.
47. Teitelbaum I, and J. B. Peritoneal Dialysis. Am J Physiol 42(5): 1082-1096, 2003.
48. Tsai Y-C, Jeng C-R, Chang C-C, Hsiao S-H, Chang H-W, Lin C-M, Chia M-Y, Wan C-H, and Pang VF. Differences in the Expression of Innate Immune Response-Modulating Genes in Blood Monocytes between Subclinically Porcine Circovirus Type 2 (Pcv2)-Infected and Pcv2-Free Pigs Prior to and after Lipopolysaccharide Stimulation in



doi:10.6342/NTU201903182

Vitro. Taiwan Veterinary Journal 40: 37-48, 2014.
49. Van Biesen W, Vanholder R, and N. L. Animal models in peritoneal dialysis: a story of kangaroos and ostriches. Peritoneal dialysis international : journal of the International Society for Peritoneal Dialysis 26: 571-573, 2006.
50. Walters EM, Wolf E, Whyte JJ, Mao J, Renner S, Nagashima H, Kobayashi E, Zhao J, Wells KD, Critser JK, Riley LK, and RS. P. Completion of the swine genome will simplify the production of swine as a large animal biomedical model. BMC Med Genomics 15: 55, 2012.
51. Wang L, He FL, Liu FQ, Yue ZD, and Zhao HW. Establishment of a hepatic cirrhosis and portal hypertension model by hepatic arterial perfusion with 80% alcohol. World J Gastroenterol 21: 9544-9553, 2015.
52. Wang L, Liu N, Xiong C, Xu L, Shi Y, Qiu A, Zang X, Mao H, and Zhuang S. Inhibition of EGF Receptor Blocks the Development and Progression of Peritoneal Fibrosis. Journal of the American Society of Nephrology : JASN 27: 2631-2644, 2016.
53. Wang L, and Zhuang S. The Role of Tyrosine Kinase Receptors in Peritoneal Fibrosis. Peritoneal dialysis international : journal of the International Society for Peritoneal Dialysis 35: 497-505, 2015.
54. Yáñez-Mó M, Lara-Pezzi E SR, Ramírez-Huesca M, Domínguez-Jiménez C, Jiménez-Heffernan JA, Aguilera A, Sánchez-Tomero JA, Bajo MA AV, Castro MA, del Peso G, Cirujeda A, Gamallo C, Sánchez-Madrid F, and M. L-C. Peritoneal Dialysis and Epithelial-to- Mesenchymal Transition of Mesothelial Cells. The New England Journal of Medicine 348: 2003.
55. Zhou Q, Bajo MA, Del Peso G, Yu X, and Selgas R. Preventing peritoneal membrane fibrosis in peritoneal dialysis patients. Kidney Int 90: 515-524, 2016.



doi:10.6342/NTU201903182